Bioactive Materials 22 (2023) 274–290

Contents lists available at ScienceDirect

Bioactive Materials

journal homepage: www.keaipublishing.com/en/journals/bioactive-materials

A shear-thinning, ROS-scavenging hydrogel combined with dental pulp stem cells promotes spinal cord repair by inhibiting ferroptosis☆

Yibo Ying [a,b,1], Zhiyang Huang [a,b,1], Yurong Tu [a,b,1], Qiuji Wu [a,b,1], Zhaoyu Li [f], Yifan Zhang [a,b], Huilei Yu [a,b], Annian Zeng [a,b], Hanzhi Huang [a,b], Jiahui Ye [a,b], Weiyang Ying [a,b,c], Min Chen [a,b], Zhiyi Feng [a,b], Ziyue Xiang [a,b], Qingsong Ye [d,e,***], Sipin Zhu [a,b,*], Zhouguang Wang [a,b,**]

[a] School of Pharmaceutical Science, Wenzhou Medical University, Wenzhou, Zhejiang, 325000, China
[b] Department of Orthopaedics, The Second Affiliated Hospital and Yuying Children's Hospital of Wenzhou Medical University, Wenzhou, Zhejiang, China
[c] Department of Pain Medicine, The Second Affiliated Hospital and Yuying Children's Hospital of Wenzhou Medical University, Wenzhou, 325000, Zhejiang, China
[d] Center of Regenerative Medicine, Renmin Hospital of Wuhan University, Wuhan, 460030, Hubei, China
[e] Massachusetts General Hospital, Harvard University, Boston, 02114, USA
[f] Department of Overseas Education College, Jimei University, Xiamen, Fujian, China

ARTICLE INFO

Keywords:
Shear-thinning hydrogel
Dental pulp stem cells
Ferroptosis
ROS-Scavenging
Synaptic regulation

ABSTRACT

Spinal cord injury (SCI) is a serious clinical disease. Due to the deformability and fragility of the spinal cord, overly rigid hydrogels cannot be used to treat SCI. Hence, we used TPA and Laponite to develop a hydrogel with shear-thinning ability. This hydrogel exhibits good deformation, allowing it to match the physical properties of the spinal cord; additionally, this hydrogel scavenges ROS well, allowing it to inhibit the lipid peroxidation caused by ferroptosis. According to the *in vivo* studies, the TPA@Laponite hydrogel could synergistically inhibit ferroptosis by improving vascular function and regulating iron metabolism. In addition, dental pulp stem cells (DPSCs) were introduced into the TPA@Laponite hydrogel to regulate the ratios of excitatory and inhibitory synapses. It was shown that this combination biomaterial effectively reduced muscle spasms and promoted recovery from SCI.

1. Introduction

Spinal cord injury (SCI) is a serious clinical disease [1,2]. Although many studies have been carried out in past decades, no treatment that effectively achieves clinical SCI recovery has been identified [3,4]. The main goals in the treatment of SCI include the following: 1). promoting the regeneration of neurons and axons; 2). inhibiting the formation of glial scars and 3). regulating the spinal microenvironment [5,6]. Thus, a more comprehensive treatment for SCI needs to be developed.

Since neurons cannot be renewed after SCI, exogenous neuron supplementation is necessary. In 2000, Gronthos et al. identified a type of cell that had an immune phenotype that was very similar to that of bone marrow mesenchymal stem cells; this cell type can undergo self-renewal and differentiation into multiple cell types [7]. These fibroblasts are isolated from pulp tissue and are called dental pulp stem cells (DPSCs). DPSCs can undergo multidirectional differentiation. After treatment with different cytokines, DPSCs can differentiate into blood vessels, nerves and other cell types [8–10]. In addition, DPSCs have other advantages including the following: 1). DPSCs are readily available from abundant sources because the teeth that are naturally lost by children aged 6–11 years and wisdom teeth that need to be extracted from adults are rich in DPSCs; and 2). DPSCs share many common features with mesenchymal stem cells. The low immunogenicity of DPSCs and their minimal impact on the regulation of immune function allow them to be used without strict matching. Furthermore, allotransplantation of DPSCs does not cause strong rejection [11,12]. Therefore, we selected DPSCs as a supplementary source of exogenous neurons for the treatment of SCI.

☆ Yibo Ying, Zhiyang Huang, Yurong Tu and Qiuji Wu contributed equally to this work.Peer review under responsibility of KeAi Communications Co., Ltd.

* Corresponding author. Department of Orthopaedics, The Second Affiliated Hospital and Yuying Children's Hospital of Wenzhou Medical University, Wenzhou, Zhejiang, China.
** Corresponding author. School of Pharmaceutical Science, Wenzhou Medical University, Wenzhou, Zhejiang, 325000, China.
*** Corresponding author. Center of Regenerative Medicine, Renmin Hospital of Wuhan University, Wuhan, 460030, Hubei, China.
E-mail addresses: qingsongye@hotmail.com (Q. Ye), sipinzhu@163.com (S. Zhu), wzhouguang@gmail.com (Z. Wang).
[1] Equal contribution.

https://doi.org/10.1016/j.bioactmat.2022.09.019
Received 12 July 2022; Received in revised form 8 September 2022; Accepted 18 September 2022

Abbreviations

4HNE	4-hydroxynonenal
ASCL1	achaete-scute complex homolog 1
BCA	bicinchoninic acid
BMS	basso mouse scale
BSA	bovine serum albumin
CCK8	Cell Counting Kit-8
CNS	central nervous system
DPBS	Dulbecco's phosphate-buffered saline
DPSCs	dental pulp stem cells
EMG	electromyogram
FBS	fetal bovine serum
FPN	ferroportin
FTH	ferritin heavy chain
FTL	ferritin light chain
GABA	gamma-aminobutyric acid
GPX4	glutathione peroxidase 4
HRP	horseradish peroxidase
MEPs	motor evoked potentials
NF200	neurofilament 200
NOX2	nADPH oxidase 2
PBS	phosphate-buffered saline
PVDF	polyvinylidene fluoride
RIPA	radioimmunoprecipitation assay
ROI	region of interest
ROS	reactive oxygen species
SCI	spinal cord injury
SD	standard deviation
TAM	tibialis anterior muscle
TBST	Tris-buffered saline with Tween
TFR	transferrin receptor
TPA	N1-(4-boronobenzyl)-N3-(4-boronophenyl)-N1, N1, N3, N3-tetramethylpropane-1,3-diaminium
VGAT	vesicular GABA transporter
WB	western blotting

After SCI, toxic substances, such as excitatory neurotransmitters and oxygen free radicals, are released, forming a local microenvironment that is not conducive to the survival of transplanted stem cells [13,14]. To protect stem cells from this toxic microenvironment, a bioactive material that can remove reactive oxygen species was used. A shear-thinning hydrogel is a kind of hydrogel that can be transformed from the gel state to flow state after exposure to shear force [15,16]. Because of its soft texture and good deformability [17], this type of hydrogel is particularly suitable for soft tissue applications (e.g., spinal cord) [18]. In addition, the gel-sol transformation only occurs at the interface between the needle wall and the hydrogel, ensuring the intact structure of the internal hydrogel [19]. At present, the mechanisms underlying the gelling of shear-thinning hydrogels mainly include hydrogen bonding, hydrophobic interactions and ion interaction forces [20,21]. Laponite (production type: XLG) ($Na^{+0.7}[(Si_8Mg_{5.5}Li_{0.3})O_{20}(OH)_4]^{-0.7}$) is a kind of flake-like nanoparticle with a positive charge on its edge and a negative charge on its surface [22]. Because it has good biocompatibility and can be degraded into nontoxic bioabsorbable minerals, laponite has been used in the food, medicine and cosmetics industries. In terms of gelling, laponite easily forms shear-thinning hydrogels with various biopolymers because of its large surface area and surface charge [23]. Similar to covalently cross-linked hydrogels, shear-thinning hydrogels are injectable, but no trigger is required to initiate the chemical reaction of the gel in situ, reducing the possibility of producing tissue-toxic substances [24,25]. N^1-(4-boronobenzyl)-N^3-(4-boronophenyl)-N^1, N^1, N^3, N^3-tetramethylpropane-1,3-diaminium (TPA) is a good reactive oxygen species (ROS) scavenger that is effective in reducing oxidation in damaged tissues [26,27]. On the other hand, TPA can combine with a variety of chemicals to form hydrogels while retaining its antioxidant effects; additionally, clinical antioxidant drugs can be encapsulated in hydrogels, which serves as carriers for these drugs. The unique nature of TPA eliminates concerns about issues related to drug release. Therefore, in this study, we combined the positively charged TPA with the negatively charged Laponite to generate a shear-thinning hydrogel, which was used to encapsulate and protect DPSCs.

In recent years, a type of cell death that is mediated by iron ions has been discovered, and it is called ferroptosis [28,29]. This type of cell death is caused by the entry of excessive amounts of iron ions into cells and the subsequent induction of a Fenton reaction, which leads to the production of lipid peroxides or GPX4 due to the disruption of the reductase system [30,31]. Recent studies have reported changes in iron levels in patients with CNS injury. Due to the vascular rupture caused by SCI, blood cells are deposited at the site of injury. A large number of free iron ions are subsequently released due to the death and breakdown of blood cells, leading to an imbalance in iron homeostasis [32]. Ferroptosis, caused by iron overload, leads to increased lipid ROS synthesis, cell death, synaptic retraction and scar hyperplasia. Therefore, we sought to verify whether TPA@laponite shear-thinning hydrogels with ROS-scavenging ability combined with DPSCs can regulate iron metabolism and further inhibit ferroptosis.

In general, this study aimed to use a TPA@laponite shear-thinning hydrogel and DPSCs to achieve the multifactor-mediated coordinated regulation of the spinal cord microenvironment and nerve regeneration to promote the overall recovery from SCI.

2. Materials and methods

2.1. Reagents and antibodies

Details are provided in Supplementary Tables 1 and 2

3. Construction and characterization of hydrogels

3.1. Synthesis and identification of TPA

One gram of N,N,N′,N′-tetramethyl-1,3-propylenediamine and 5 g of 4-(bromomethyl) phenyboric acid were dissolved in 100 mL dimethylformamide, stirred for 24 h at 60 °C, and then washed with tetrahydrofuran 5 times [33]. 1H nuclear magnetic resonance spectra of TPA in D_2O were obtained by Zhongke-Niuji WNMR-1-400MHz (400 MHz) [27].

3.2. Preparation of the TPA@laponite shear-thinning hydrogel

Laponite powder was dispersed in deionized water under magnetic agitation to prepare 20, 50, and 100 mg/mL Laponite dispersions. TPA (25 mg) was dissolved in 1.0 mL of deionized water and mixed with an equal volume of a Laponite dispersion to promote the formation of a TPA@laponite shear-thinning hydrogel. The final concentration of TPA was 12.5 mg/mL, and the final concentrations of Laponite were 10, 25, and 50 mg/mL.

3.3. Determination of hydrogel properties

3.3.1. Rheological assessment of the hydrogel

The rheology of the hydrogel was investigated with a Thermo Fisher HAAKE MARS rheometer. A 35 mm plate was used, and the plate

clearance was set to 1 mm. A strain sweep rheological test was performed on the TPA@laponite shear-thinning hydrogel, and this test was carried out from 0.1% to 500% strains at 25 °C at a fixed frequency of 1 Hz; a frequency sweep rheological test was performed on the TPA@laponite shear-thinning hydrogel, and this test was carried out from 1 to 100 Hz at a fixed strain of 1% at 25 °C; a time sweep rheological test was performed on the TPA@laponite shear-thinning hydrogel, and this test was performed at a fixed frequency and strain of 1 Hz and 1%, respectively, at 25 °C for 10 min.

3.3.2. Scanning electron microscopy of the TPA@laponite shear-thinning hydrogel

The micromorphology of the TPA@laponite shear-thinning hydrogel was determined using scanning electron microscopy (SEM, Nova 200 NanoSEM, FEI, USA). In short, hydrogel samples were dried in liquid nitrogen, brittle broken, and dried in a lyophilizer. Before the experiments, the samples were coated with a thin layer of gold under a vacuum using a Desk II gold sputter coater (Denton Vacuum, Morristown, NJ) for 60 s.

3.3.3. Measurement of the zeta potentials of the materials

The zeta potentials were measured at 25 °C in water by using a Malvern Zetasizer Nano ZSP instrument (Nano-ZS90) equipped with a Malvern surface zeta potential cell.

3.3.4. Degradation of the hydrogel

A experiment to assess the degradation of the TPA@laponite shear-thinning hydrogel in PBS solution was carried out to confirm the degradation properties of this hydrogel *in vitro*. In brief, 300 μL of the TPA@laponite shear-thinning hydrogel was added to a 1.5 mL Eppendorf tube, and then, 1 mL of PBS solution was added. Hydrogels were harvested at different intervals, and the surface liquid was removed with filter paper. Then, the hydrogels were weighed, and the weights were recorded.

In vivo imaging experiments. First, the TPA@laponite shear-thinning hydrogel was labeled with the fluorescent dye Cy5 (excitation wavelength 580 nm, emission wavelength 640 nm). The model of hydrogel degradation in skin was first established by injecting 50 μL of the hydrogel into the back skin of healthy C57BL/6 mice. *In vivo* imaging was performed on 0 d, 1 d, 3 d, 7 d, 14 d, and 21 d to observe the distribution of fluorescence in the injected site.

3.4. 3D cell culture

Digested DPSCs were collected and centrifuged at 1000 rpm for 3 min, the supernatants were removed, and the cells were resuspended in complete medium. After counting, 10^6 cells were transferred to a 15 mL centrifuge tube, and the volume of complete medium was adjusted to 1 mL. After adding 25 mg TPA, the solution was quickly dissolved by pipetting, and then, 1 mL of a 50 mg Laponite dispersion was added and gently stirred until it was evenly mixed. Finally, 4 mL of complete medium was added, and the cells were cultured for 24 h in a cell incubator. At the end of the culture, the upper layer of medium was carefully aspirated, and then, the lower layer of the hydrogel/cell coculture system was aspirated to measure cell viability with a calcium-AM/PI kit. Normal cells cultured in Petri dishes were used as a control, and their viability was examined at the same time as the 3D cultured cells.

3.5. Isolation of DPSCs and cell culture

DPSCs were isolated from volunteers who were recruited by the Department of Oral Maxillofacial Surgery, Stomatological Hospital of Wenzhou Medical University. The donors (20–35 years old, n = 3) had no lesions in the periodontal and apical period of the third molars, and they had no dental caries. This project was approved by the ethics department (Case No. WYKQ2018008SC). Dental pulp was removed from the teeth, cut into 1 mm^3 pieces, and then washed with PBS containing antibiotics. Then, the tissues were treated with 4 mg/mL dispase (Sigma–Aldrich, USA) and 3 mg/mL type I collagenase (Gibco, USA) at 37 °C for 30 min. The cells were suspended and cultured at 37 °C in a primary mesenchymal stem cell culture system. Five days later, the culture medium was discarded and replaced with fresh medium; this was repeated every two days. Immunofluorescence was used to identify DPSCs. Primary astrocytes and NSC34 cells were cultured in high-glucose DMEM supplemented with 100 μg/mL streptomycin, 100 U/mL penicillin and 10% FBS in a 37 °C incubator with 5% CO_2.

3.6. CM-DiI staining of DPSCs

DPSCs were centrifuged at 1000 rpm for 5 min, and the supernatants were discarded. The cells were resuspended in Dulbecco's phosphate-buffered saline (DPBS) at a density of 1×10^6 cells/mL. CM-DiI (concentration: 1 mg/mL) was added and gently mixed with the cells for 30 s. The cells were incubated at 37 °C for 5 min and subsequently incubated at 4 °C for 15 min. Finally, the free staining solution was removed by washing three times with DPBS. The whole process was performed in the dark.

3.7. Assembly of the TPA@laponite shear-thinning hydrogel combined with DPSCs

CM-DiI-stained DPSCs were centrifuged, and the supernatants were discarded. Then, 1×10^6 DPSCs were resuspended in 1 mL TPA solution (25 mg/mL), and 1 mL Laponite suspension (50 mg/mL) was added to obtain the TPA@Laponite hydrogel combined with DPSCs. The final concentrations of TPA and Laponite in the hydrogel were 12.5 mg/mL and 25 mg/mL, respectively.

4. Cell stimulation

When CCK8 was used to investigate the toxicity of the hydrogel and its components, 10^4 DPSCs/well were seeded in 96-well plates. In the TPA concentration selection experiment, basal media supplemented with 3.125 μg/mL, 6.25 μg/mL, 12.5 μg/mL and 25 μg/mL TPA were prepared. The corresponding basal media supplemented with TPA were used to replace the media after cell adherence. The medium in the control group was replaced with fresh basal media. To determine the toxicity of the hydrogels and their components, basal media supplemented with 12.5 μg/mL TPA, 25 μg/mL Laponite, and 1 μL/mL TPA@Laponite hydrogels were prepared. The corresponding basal media were used to replace the media after cell adherence, and the medium in the control group was replaced with fresh basal media. The corresponding indices were assessed after 24 h of culture (SFig. 1).

When hydrogel toxicity was observed by the Calcein-AM/PI method, 10^5 DPSCs, astrocytes and NSC34 cells per well were seeded in 12-well plates. After cell adhesion, the cells were divided into two groups. In the Gel group: TPA@Laponite hydrogel was added at a final concentration of 1 μL/mL; in the Control group: equal amounts of PBS were added. Then, the cells were placed in the incubator for further culture for 24 h, and the survival of the cells was determined (Fig. 2A–C).

A reactive oxygen probe, 4HNE immunofluorescence assays, and Calcein-AM/PI staining were used to investigate the abilities of the TPA@Laponite hydrogel to scavenge ROS and regulate ferroptosis. To that end, 10^5 cells DPSCs, astrocytes and NSC34 cells per well were plated in 12-well plates. After cell adherence, the cells were divided into three groups. In the Erastin group, medium supplemented with 5 μM Erastin was added; in the Erastin + Gel group, medium supplemented with 5 μM Erastin and 1 μL/mL TPA@Laponite hydrogel was added. In the control group, the medium was replaced with fresh basal medium. The corresponding indices were assessed after 24 h of culture (Fig. 2D–I).

When the cell confluence reached 70–80%, the level of lipid

peroxidation in the neurons was measured by WB. The cells were divided into five groups. In the Erastin group, medium supplemented with 5 μM Erastin was added. In the Erastin + Gel group, medium supplemented with 5 μM Erastin and 1 μL/mL TPA@Laponite hydrogel was added. In the $FeCl_3$ group, medium supplemented with 10 μM $FeCl_3$ was added. In the $FeCl_3$+Gel group, medium supplemented with 10 μM $FeCl_3$ and 1 μL/mL TPA@Laponite hydrogel was added. The medium in the control group was replaced with fresh basal medium. The corresponding indices were assessed after 24 h of culture (SFigs. 3 and 6).

5. Cell counting kit-8 test

Cells were incubated in 96-well plates in an incubator for 12 h, and then, the medium was aspirated. Fresh medium (90 μL) was added to each well, 10 μL CCK8 solution was added, and then, the plates were incubated in the incubator for 1 h. The absorbance was measured at 450 nm using a microplate reader (SpectraMax M2, Molecular Devices, CA, USA), and the data were processed by Prism software to generate statistical charts.

6. Calcein-AM/PI staining

A working solution with a Calcein-AM concentration of 2 μM and a PI concentration of 4.5 μM was prepared using a Calcein-AM/PI kit. After the supernatants were removed from cells cultured in the 12-well plates, the cells were washed with the assay buffer provided with the kit 3 times, 200 μL of working solution was added to each well, and the cells were incubated in an incubator for 30 min. After the free staining solution was removed by washing three times with assay buffer, the cells were observed under a fluorescence microscope (Eclipse Ti–S, Nikon, Japan).

7. Neuron-induced differentiation

DPSCs were placed in 6-well plates at a density of 10^4 cells/well. The cells were randomly divided into two groups: 1). in the control group, the differentiation of DPSCs was induced by neuron-induced differentiation medium (DMEM-high glucose supplemented with 100 nM dexamethasone, 50 μg/mL ascorbic acid-2-phosphate, 50 μM indomethacin, 10 μg/mL insulin, and 0.45 mM 3-isobutyl-1-methylxanthine) [34]; and 2). in the TPA group, the differentiation of DPSCs was induced by neuron-induced differentiation medium in the presence of 1 μL/mL TPA@laponite hydrogel. The medium was changed every 2 days, and differentiation was induced for 6 days. After the induction of differentiation, immunofluorescence was used to assess cell characteristics.

8. SCI mouse model

Adult female C57BL/6 mice (20–23 g, n = 120) were obtained from Charles River Laboratories. The care and use of all the animals conformed to the guidelines set forth by the Chinese National Institutes of Health, and protocols involving animals were approved by the Animal Care and Use Committee of Wenzhou Medical University (No. WYDW-2018-0342). C57BL/6 mice were anesthetized with 1% pentobarbital. The spinal cord was exposed after the T9-T10 spinous and laminoid processes were removed. The spinal cord was contused in the T9 position by a weight (10 g) from a height of 5 cm. Cefazolin sodium (0.9%) was injected into the peritoneal cavity of the mice twice daily, and artificial assisted urination was performed every morning and evening [35].

9. Hydrogel injection

C57BL/6 mice were divided into 5 groups with 24 mice in each group: 1). the Sham group, 2). the SCI group, 3). the Gel group (TPA@laponite shear-thinning hydrogel was injected) and 4). the Gel + DPSC group (TPA@laponite shear-thinning hydrogel combined with DPSCs was injected). After spinal cord shock injury was applied, 10 μL hydrogel/cell suspension was injected into the center and four corners of the damaged area (2 μL at each point) of the mice in the Gel group, Gel + DPSC group and DPSC group at a rate of 0.5 μL/min. After the injection, the needle remains at the injection site for 3 min to prevent outflow, and then, the needle was slowly removed. The Sham group and the SCI group were injected with the same volume of saline. The mice were injected intraperitoneally (i.p.) with cyclosporine (10 mg/kg) to achieve immunosuppression every day after transplantation.

10. Evaluation of the functional recovery of mice with SCI

The BMS score, footprints and video recording images were used to evaluate the function of the spinal cord. The mice were allowed to move freely on a platform. The BMS scores were evaluated according to hind limb walking and limb movement. The mice were placed in a plastic film-covered 5 cm × 50 cm track to ensure their adaptation to the dark environment. The mice were allowed to move from the starting point to the end in the track, and their hind was marked with red dye. Motile function was evaluated according to footprints. Video images were recorded to analyze weight support, leg extensor spasms, and foot posture [36].

11. Electrophysiological assessments of hindlimb motor function

MEPs were induced according to a previously described method [37,38]. The mice were briefly anesthetized with 1% sodium pentobarbital. The stimulating needle electrode (DSN1620, Medtronic, USA) acted as an anode and was inserted under the skin at the base of the nose, with the tip touching the scalp. The needle electrode acted as a cathode and was placed at the midpoint of the subcutaneous ear. Recording electrodes were inserted into the tibialis anterior muscle (TAM). A ground electrode was placed under the skin at the bottom of the tail. A pulse of electrical stimulation (10 mA, 0.1 ms, 1 Hz) was passed through a stimulator (Keypoint, Medtronic, USA) to stimulate the brain. The electrical stimulation was repeated six times at 15-s intervals in each mouse. The amplitude of each evoked potential after a single stimulus was recorded.

12. Hematoxylin and eosin (H&E) staining

Tissues were harvested from mice in each group for pathologic analysis. The tissues were fixed with 4% paraformaldehyde, embedded in paraffin and then cut into 5 μm thick sections for H&E staining. After dewaxing and rehydration with gradient ethanol, the sections were stained with hematoxylin for 6 min, differentiated with differentiation solution for 3 min, washed twice with running water for 2 min each, and then stained with eosin for 2 min. Ethanol and xylene were used for dehydration and clearing, and the sections were sealed with neutral resin. Then, the stained sections were examined under an optical microscope.

13. Nissl staining

Nissl dye was used to label Nissl bodies in neurons. The tissue sections were dewaxed, rehydrated and stained with tar violet. After incubation at 56 °C for 60 min, the sections were washed with distilled water and 95% alcohol. Subsequently, dehydration, clearing and sealing were performed. An optical microscope was used to observe the sections and capture images.

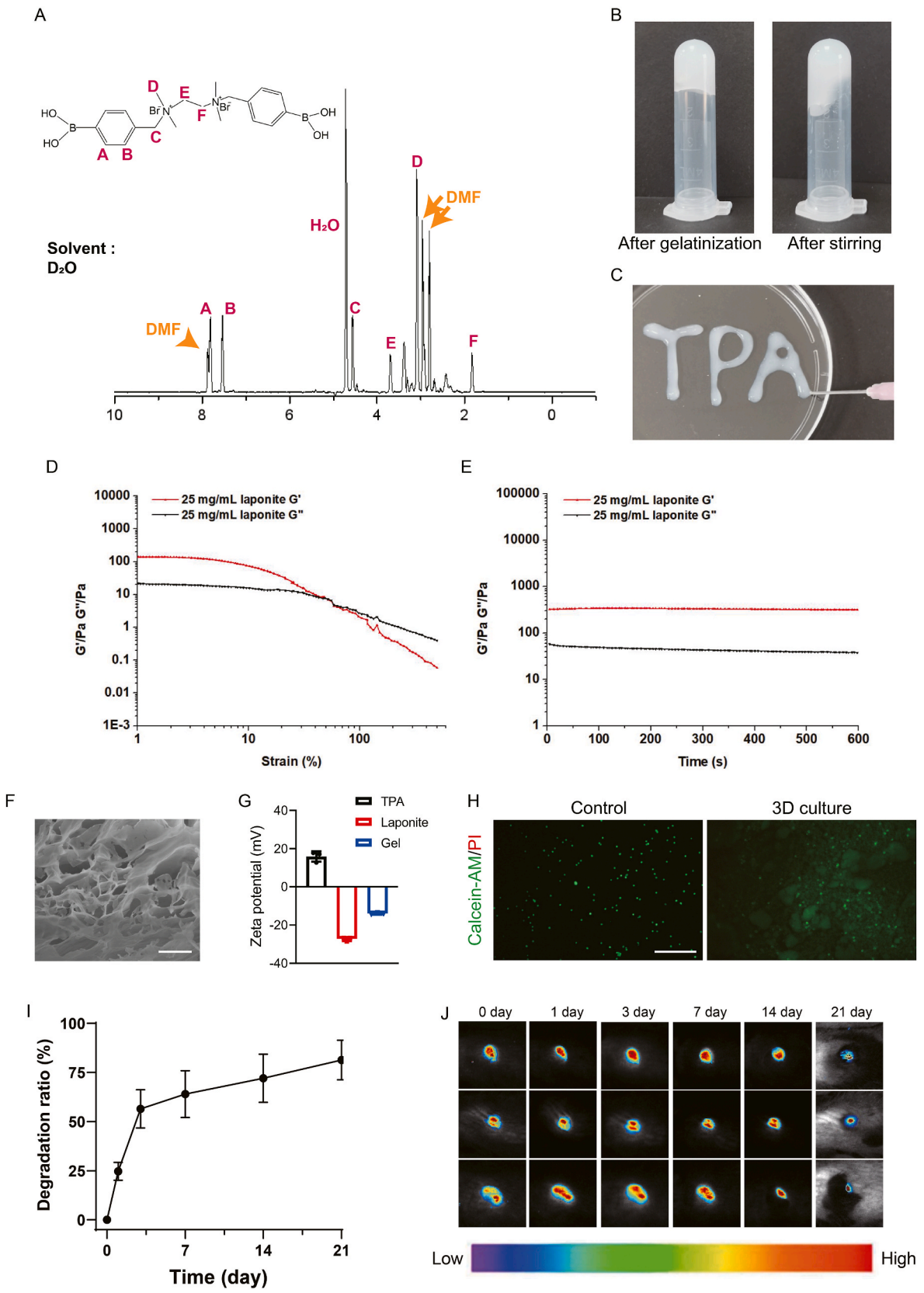

Fig. 1. Characterization of the TPA@lapnoite shear-thinning hydrogel.
(A) ^{1}H NMR (300 MHz, in D_2O) spectrum of the TPA@lapnoite shear-thinning hydrogel. **(B)** Photographs of the hydrogel. **(C)** Demonstration of excellent injectability of the hydrogel. **(D)** Oscillating time-sweep measurements. (**E**) Strain-sweep measurements. (**F**) SEM image of the hydrogel; scale bar: 10 μm. (**G**) Zeta potentials of the hydrogels and their components. (**H**) Assay of cell activity after the 3D culture of cells and the hydrogel. (**I**) *In vivo* spectrum imaging system (IVIS) images of the retention of the hydrogel *in vivo*. (**J**) Statistical analysis of the *in vitro* degradation results on 0 d, 1 d, 3 d, 7 d, 14 d, and 21 d.

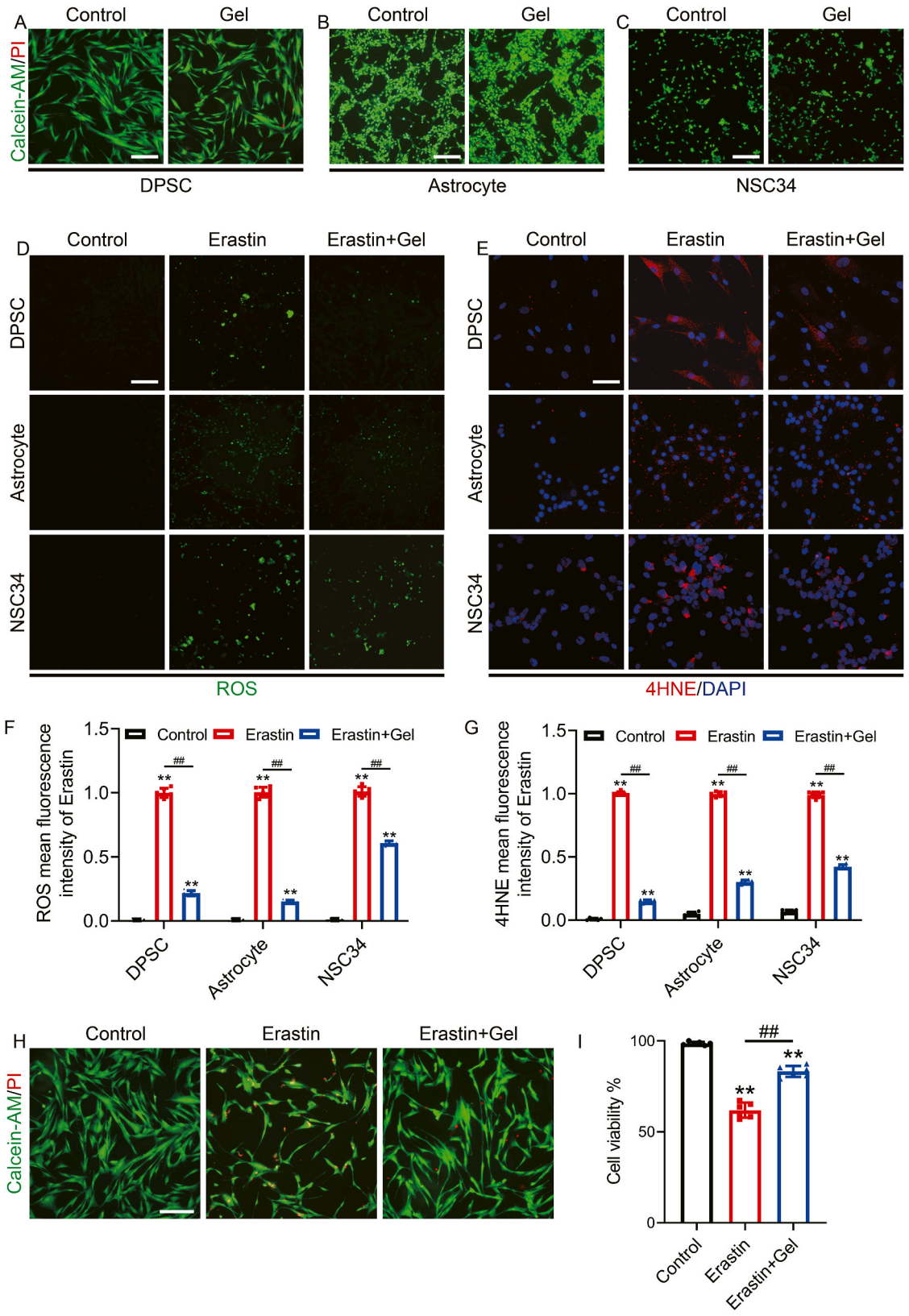

Fig. 2. The TPA@laponite shear-thinning hydrogel scavenges ROS and inhibits lipid peroxidation *in vitro*
(A- C) Immunofluorescence staining of Calcein-AM (green) and PI (red) in DPSCs, astrocytes, and NSC34 cells in the control and gel groups. Magnification: 20X; scale bar: 100 μm. **(D)** Immunofluorescence staining of ROS (green) in DPSCs, astrocytes, and NSC34 cells in the control, Erastin and Erastin + gel groups. Magnification: 20X; scale bar: 100 μm. **(E)** Immunofluorescence staining of 4HNE (red) and DAPI (blue) in DPSCs, astrocytes, and NSC34 cells in the control, Erastin and Erastin + gel groups. Magnification: 20X; scale bar: 100 μm. **(F)** Statistical analysis of ROS expression in each group. **(G)** Statistical analysis of 4HNE expression in each group. **(H)** Immunofluorescence staining of Calcein-AM (green) and PI (red) in the control, Erastin and Erastin + gel groups. Magnification: 20X; scale bar: 100 μm. **(I)** Cell viability of each group. ** represents $P < 0.01$ vs. the control group. ## represents $P < 0.01$. The data are expressed as the mean values ± SDs ($n = 6$).

14. Perls staining

Perls staining labels iron ions in tissue. After dewaxing and rehydration, the tissues were incubated with Perls solution for 30 min. After washing with distilled water for 5 min, the organization fibers were stained with eosin for 15–30 s and then rinsed with tap water. An optical microscope was used to observe the sections and captures images.

15. Western blotting analysis

Extracted tissue was stored at −80 °C for Western blotting. The tissues were homogenized in modified radioimmunoprecipitation assay (RIPA) buffer supplemented with 10 μL/mL protease inhibitor cocktail. The extracts were then centrifuged at 12,000 rpm, and the supernatants were collected for protein assays. The protein concentrations were quantified with bicinchoninic acid (BCA) reagents. Forty micrograms of protein per lane was loaded onto 12% and 10% gels for electrophoresis. The proteins were electrophoretically transferred to PVDF membranes. Then, the membranes were blocked with 5% skim milk for 2 h and incubated with primary antibodies at 4 °C overnight. After washing with TBST three times, the membranes were incubated with HRP-conjugated secondary antibodies at room temperature for 2 h. The ChemiDoc XRS + Imaging System (Bio-Rad) was used to measure the signal. ImageJ software was used to measure and quantify the band densities.

16. Immunofluorescence staining

The sections were dewaxed and rehydrated. After antigen repair, the tissues were sealed with 5% bovine serum albumin (BSA) for 30 min. The slides were incubated overnight with the indicated primary antibodies at 4 °C and then incubated with a corresponding fluorescently labeled secondary antibody for 1 h. The nuclei were stained using DAPI. A Nikon Ti-E&A1 plus microscope was used for image acquisition. All fluorescent images were captured at the junction between the injured and uninjured areas. Fluorescence images were captures from the regions of interest (ROIs) in different groups. The cell count function of ImageJ was used to count the number of cells, and the fluorescence intensity within the cells was calculated by using ImageJ after the target cells were delineated. Six samples from each group were used for image acquistion. Prism 7 (GraphPad, San Diego, CA) was used to generate the statistical graphs.

17. Statistical analysis

BMS scores were analyzed using generalized linear mixed models. Two-sided Student's *t*-test was used to compare data between two groups. Analysis of variance and Tukey's post-hoc analyses were used to compare data from more than two groups. Statistical analysis was performed using Excel and GraphPad Prism 7. The data are displayed as the mean ± standard deviation (SD). $P < 0.05$ indicates a significant difference.

18. Results

18.1. Characterization of the TPA@laponite shear-thinning hydrogel

The successful synthesis of TPA was confirmed by hydrogen nuclear magnetic resonance spectroscopy (Fig. 1A). Then, the toxicity of TPA was examined, and the CCK8 results showed that TPA exerted slight toxic effects at concentrations as low as 12.5 μg/mL (Sfigure 1A). The TPA@lapnoite shear-thinning hydrogel was formed by mixing TPA and laponite, and then, the mixture was allowed to stand to form the gel. When the gel was stirred, the hardness of the gel decreased (Fig. 1B). The hydrogel exhibited good injectability (Fig. 1C). The toxicity of the TPA@Laponite hydrogel and its components was examined. The results showed that the minimal toxicity of 12.5 μg/mL TPA was neutralized after hydrogel formation, and the cells grew well (Sfigure 1B). To further explore why the toxicity of TPA was neutralized, the zeta potentials of the hydrogel and its components were examined. The results showed that TPA had a strong positive charge, which affected cell proliferation and survival, while Laponite had a negative charge, which neutralized the positive charge of TPA. The resulting TPA@Laponite hydrogel was negatively charged and therefore less toxic to biological samples (Fig. 1G). To investigate the rate of gelation between components, we mixed 10, 25, and 50 mg/mL Laponite dispersion with TPA solution. Dynamic rheological measurements of gel dynamics and viscoelasticity revealed that the TPA@lapnoite hydrogel exhibited shear-thinning behavior. Oscillating time-sweep measurements showed that when the Laponite concentration was increased from 10 to 50 mg/mL, the G′ and G″ values increased from approximately 90 to 25000 Pa and 10–2000 Pa, respectively (Fig. 1D; Sfigure 2A, C). These results indicate that TPA and Laponite can quickly form a stable network structure. Such a network exhibits more elastic properties than viscous properties, and it is not disrupted under suitable shear stress conditions caused by rapidly reversible interactions. From the strain sweep results, we observed that the three hydrogels showed a steep decrease in storage ability and loss moduli after a certain yield strain, indicating material yielding (Fig. 1 E; Sfigure 2B, D). The yield strain of 50 mg/mL TPA@lapnoite hydrogel was highest, indicating that the 25 mg/mL TPA@lapnoite hydrogel may be easier to inject than the 50 mg/mL hydrogel. Based on these results, this hydrogel exhibited fast gelation and shear-thinning properties. To analyze whether the structure of the TPA@Laponite hydrogel is conducive to cell growth and migration, scanning electron microscopy was used to determine the microstructure of the hydrogel, and the experimental results showed that the hydrogel had a good void structure, which was conducive to the growth and migration of cells (Fig. 1F). Then, 3D culture of the cells and hydrogel was used to determine whether the cells could survive in the hydrogel. The experimental results showed that the cells still showed good activity after 24 h of coculture (Fig. 1H). Moreover, an *in vitro* degradation experiment was carried out with the TPA@laponite shear-thinning hydrogel. The TPA@laponite shear-thinning hydrogel was immersed in PBS solution. The hydrogel degraded by 81.28 ± 10.11% in 21 days (Fig. 1I). *In vivo* imaging was used to further evaluate the effect of the degradation of the TPA@laponite shear-thinning hydrogel *in vivo*. At different time points, the intensity and range of fluorescence were measured to monitor the changes in TPA@laponite shear-thinning hydrogel degradation *in vivo*. As shown in Fig. 1J, the fluorescence signal continuously decreased at the indicated time points. An obvious decrease in the hydrogel volume was observed over time.

In conclusion, the TPA@lapnoite hydrogel has good physical properties, such as shear-thinning ability and injectability, and can remain in the body for a long time.

18.2. The TPA@laponite shear-thinning hydrogel inhibited lipid peroxidation in vitro

After the hydrogel was successfully generated, its toxicity was first measured. The Calcein-AM/PI staining results showed that the hydrogel did not cause significant toxicity in DPSCs, astrocytes and NSC34 cells (Fig. 2A–C). Erastin is a ferroptosis agonist that reduces glutathione levels by directly inhibiting the activity of the cystine/glutamate antitransport system Xc^-, which could increase the level of lipid peroxidation in cells [39,40]. Ferroptosis activation experiments with Erastin showed significant increases in the ROS and 4HNE levels in all types of cells. The ROS and 4HNE levels were significantly decreased after hydrogel treatment (Fig. 2D–G). The Calcein-AM/PI staining results showed that erastin-induced cell death was significantly inhibited by the hydrogel (Fig. 2H–I).

In conclusion, the TPA@lapnoite shear-thinning hydrogel was successfully generated, and the hydrogel could scavenge ROS and inhibit lipid peroxidation *in vitro*.

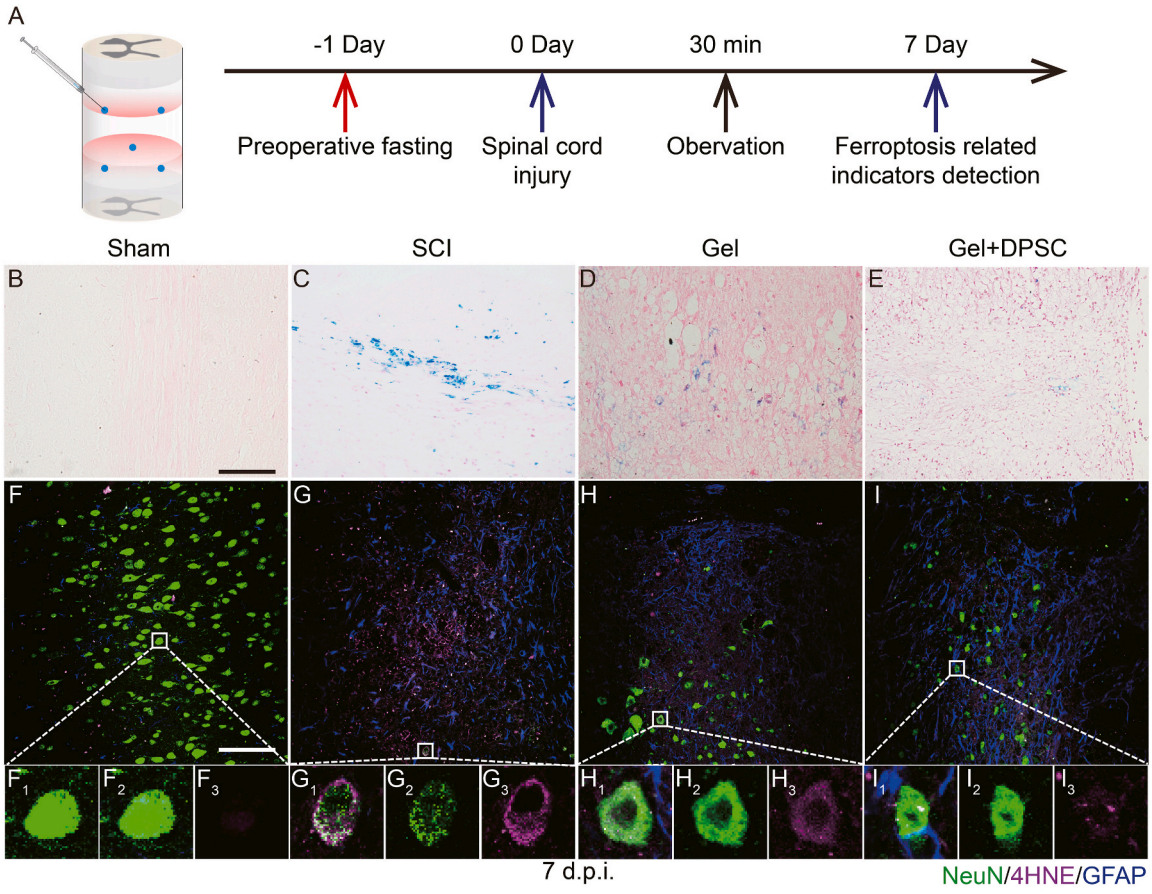

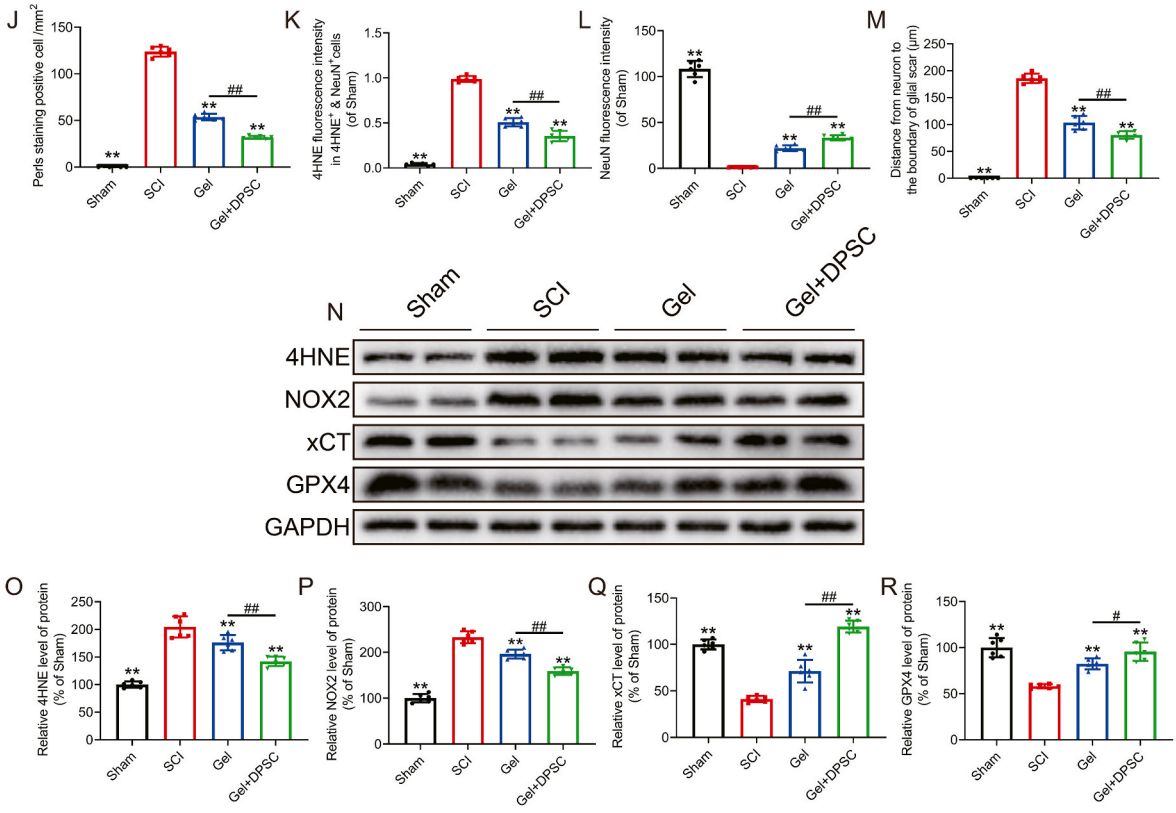

(caption on next page)

Fig. 3. The TPA@laponite shear-thinning hydrogel combined with DPSCs inhibits lipid peroxidation *in vivo*
(A) Schematic diagram of the experimental procedure for the detection of early ferroptosis. **(B–E)** Perls staining results of the Sham, SCI, Gel and Gel + DPSC groups. Magnification: 20X; scale bar: 100 μm. **(F–I)** Immunofluorescence staining of NeuN (green), 4HNE (purple), and GFAP (blue) in each group at 7 d.p.i. F_1–I_3 represent the enlarged images. F_2–I_2/F_3–I_3 represent the green and purple single-channel images of F_1–I_3, respectively. F_1–I_1 represent the merged images of each single channel. The white boxes represent the enlarged areas. Magnification: 20X; scale bar: 100 μm. **(J)** The density of Perls-positive cells in each group. **(K)** The mean fluorescence intensity of 4HNE in the neurons from each group. **(L)** The mean fluorescence intensity of NeuN in each group. **(M)** The distance between the neurons and the boundary of the glial scar in each group. **(N)** Western blotting showing the expression of 4HNE, NOX2, XCT and GPX4 in each group (tissue) at 7 d.p.i. **(O–R)** Quantitative analysis of 4HNE **(O)**, NOX2 **(P)**, xCT **(Q)** and GPX4 **(R)** protein expression. ** represents $P < 0.01$ vs. the SCI group. # represents $P < 0.05$, and ## represents $P < 0.01$. The data are represented as the mean ± SD (n = 6).

18.3. The TPA@laponite shear-thinning hydrogel combined with DPSCs inhibited lipid peroxidation in vivo

After verifying that the hydrogel scavenges ROS and inhibits lipid peroxidation *in vitro*, we sought to explore its efficacy *in vivo*. After establishing the SCI model, the hydrogel was injected into the spinal cords of the mice, and the levels of Fe^{3+}, lipid peroxides and reducing system components were measured 7 d.p.i. (Fig. 3A). The Perls staining results showed that large amounts of iron ions were produced after SCI. Hydrogel treatment reduced the level of iron ions, and the Gel + DPSC group had lower iron ion levels than the Gel group (Fig. 3B–E, J). We then used immunofluorescence to measure the levels of lipid peroxides, and we found that the expression level of 4HNE increased after SCI, especially in neurons. After hydrogel treatment, the levels of lipid peroxides in neurons decreased significantly, and hydrogel combined with DPSCs was more better effective (Fig. 3F–I, K). Inhibition of lipid peroxidation by the Gel + DPSC system improved the survival rate of neurons and promoted neurons closer to the site of injury to survive (Fig. 3F–I, L-M). To further confirm whether lipid peroxidation occurs after SCI and to elucidate the regulatory effect of the Gel + DPSC system on lipid peroxidation, we used WB to semiquantify the expression levels of relevant indicators. The results showed that after SCI, the expression levels of the oxidation promoter NOX2 and lipid peroxide 4HNE were significantly increased, the expression levels of GPX4 reduction system components were significantly inhibited, and the expression levels of xCT and GPX4 were significantly downregulated. Hydrogel treatment inhibited the production of lipid peroxidation and promoted the recovery of the GPX4 reduction system, and the Gel + DPSC system exerted a stronger effect (Fig. 3N–R). We further demonstrated the effect of the hydrogels on erastin-induced lipid peroxidation *in vitro*. The results showed that the erastin-induced upregulation of NOX2 and 4HNE was inhibited and that the disordered GPX4 reduction system was restored (SFig. 3).

To explore the expression of lipid peroxides in chronic convalescence and analyze the treatment effect of the hydrogel in tissues, we first examined the expression of lipid peroxides at 30 d.p.i. The Perls staining results showed that there was no significant difference in the content of iron ions in the tissues of each group (Sfigure 4A-D, I). Analysis of the neuronal differentiation rate of DPSCs and the distance between neurons and the site of injury showed that the hydrogel effectively improved the neuron survival rate and that DPSCs could differentiate into neurons to supplement the neuronal population at the site of injury; however, there was no significant difference in the expression of 4HNE in the neurons of each group (Sfigure 4E-H, J-L). The WB results showed that 4HNE and GPX4 expression levels were also not significantly different between groups (Sfigure 4M − O). The apparent recovery map of the spinal cord showed that the T9 segment after SCI was still transparent and thin after 30 days of treatment. In the Gel group, partial repair of the injured area was observed, but there was still a large gap compared with the normal tissue. The Gel + DPSC group exhibited the best tissue repair, and the full tissue node morphology was most similar to that of the Sham group (Sfigure 5A). H&E staining and Nessie staining of spinal cord sections showed greater neuron survival in the anterior horn of the spinal cord in the Gel group and Gel + DPSC group than in the SCI group, and there were more neurons in the Gel + DPSC group than in the Gel group (Sfigure 5B). The H&E staining of the longitudinal spinal cord showed that although the centers of the injured site of each injury group did not disappear, the range of damage and inflammatory infiltration in the Gel + DPSC group were lowest. Tissue structural integrity and neuronal survival rate were significantly higher in the Gel + DPSC group than in the SCI and Gel groups (Sfigure 5C).

In conclusion, the TPA@lapnoite shear-thinning hydrogel could inhibit lipid peroxidation and promote tissue repair *in vitro,* and the hydrogel combined with DPSCs could achieve a better therapeutic effect. Ferroptosis mainly plays an important role in the early stage of SCI and has almost no effect in the chronic recovery stage. However, the influence of ferroptosis in the early stage greatly limits recovery from SCI.

18.4. The TPA@laponite shear-thinning hydrogel combined with DPSCs inhibited ferroptosis in vitro by regulating iron metabolism

We then examined iron metabolism, another important factor in ferroptosis. TFR and FPN are important proteins that regulate the movement of iron ions into and out of cells, while ferritin, which is composed of FTH and FTL, is an important protein that stores iron ions in cells [41–43]. After SCI, the cells were exposed to a sharp increase in extracellular iron levels, increased the expression of TFR and decreased the expression of FPN to promote the intracellular transport of iron ions. The expression of FTH and FTL also increased to store a large amount of incoming intracellular iron ions. This phenomenon of iron overload is an important cause of ferroptosis [44,45]. Our results showed that TFR, FTH and FTL increased significantly in neurons after SCI, while the expression of FPN decreased significantly in neurons. After hydrogel treatment, the expression levels of TFR, FTH and FTL in neurons were significantly decreased compared with those in the SCI group, and the expression levels of FPN in neurons treated with hydrogels were significantly increased compared with those in the SCI group. The Gel + DPSC group exhibited a more significant therapeutic effect than the Gel group (Fig. 4A-T). The WB results showed that the hydrogel participated in the metabolism of iron ions *in vivo*, downregulated TFR, FTH, and FTL and upregulate FPN to reduce the pressure of iron overload in the injured spinal cord. Gel + DPSC treatment achieved a more significant therapeutic effect (Fig. 4U–Y). To further verify whether the hydrogel regulates iron metabolism, we used $FeCl_3$ to simulate the environment of iron overload *in vitro*, and the experimental results showed that the hydrogel effectively inhibited the upregulation of TFR, FTH and FTL caused by iron overload and increased the level of FPN to promote iron outflux (SFig. 6). To explore the cause of the synergism between DPSCs and the hydrogel, we examined the vascular conditions after spinal cord injury. The experimental results showed that after spinal cord injury, blood vessels exhibited disordered hyperplasia and were surrounded by fibrous scars, and the material transport function of blood vessels did not easily recover. After hydrogel treatment, scar hyperplasia was reduced, but the blood vessels were still disordered. Fibrous scarring was effectively inhibited in the Gel + DPSC group, and blood vessel regeneration became orderly after treatment with DPSCs (Sfigure 7A-C). Then, we assessed the hypoxia of the SCI group for 30 days to analyze the recovery of vascular function; the experimental results showed that the vascular function of the Gel + DPSC group was significantly improved compared with that of the Gel group and SCI group (Sfigure 7D-E).

In conclusion, the TPA@lapnoite shear-thinning hydrogel inhibited

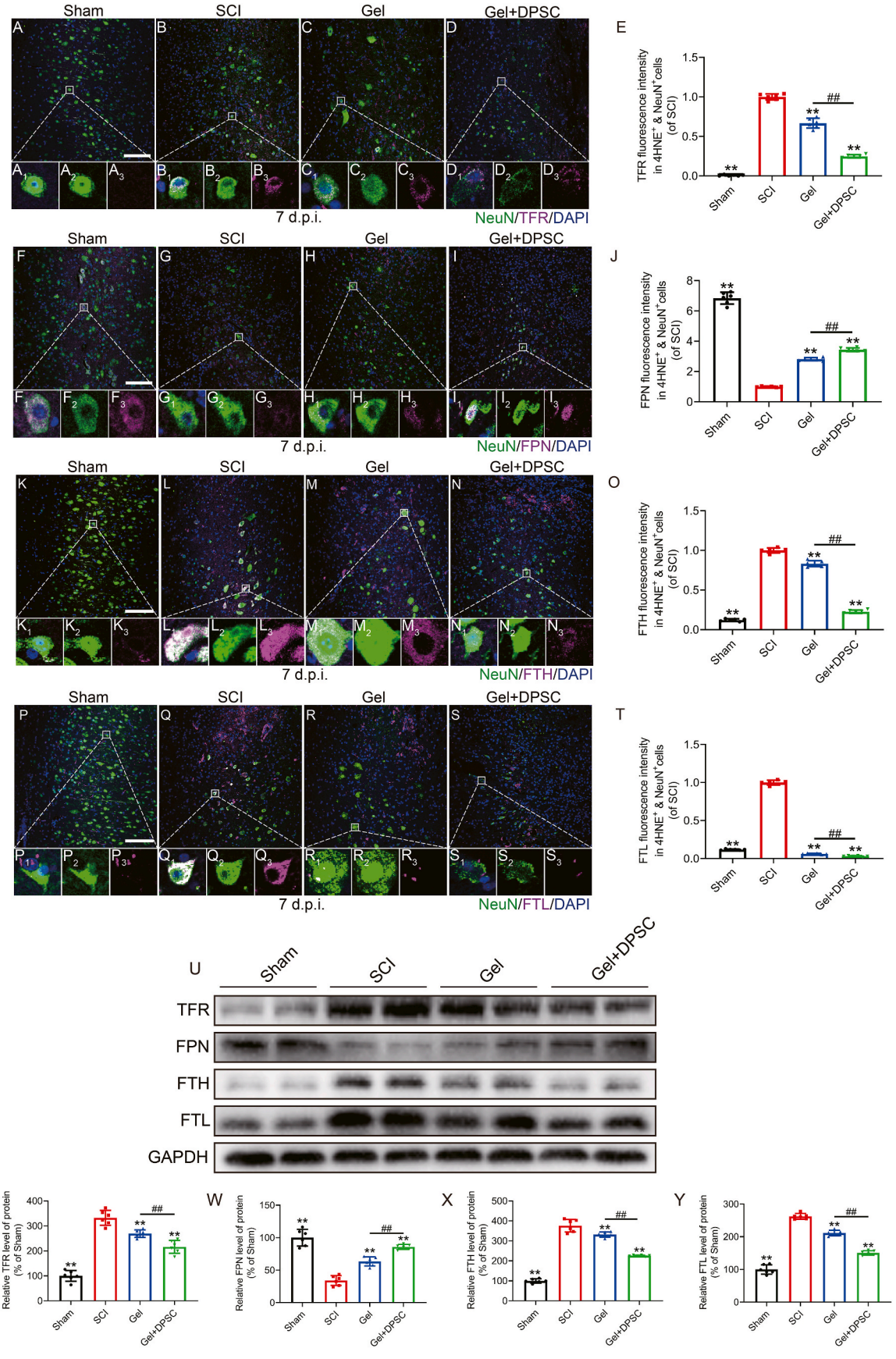

(caption on next page)

Fig. 4. The TPA@laponite shear-thinning hydrogel combined with DPSCs regulates iron metabolism *in vivo*
(A-D) Immunofluorescence staining of NeuN (green), TFR (purple), and DAPI (blue) in each group at 7 d.p.i. A_1-D_3 represent the enlarged images. A_2-D_2/A_3-D_3 represent the green and purple single-channel images of A_1-D_3, respectively. A_1-D_1 represent the merged images of each single channel. The white boxes represent the enlarged areas. Magnification: 20X; scale bar: 100 μm. **(E)** Statistical analysis of TFR expression in the neurons of each group. **(F–I)** Immunofluorescence staining of NeuN (green), FPN (purple), and DAPI (blue) in each group at 7 d.p.i. F_1–I_3 represent the enlarged images. F_2–I_2/F_3–I_3 represent the green and purple single-channel images of F_1–I_3, respectively. F_1–I_1 represent the merged images of each single channel. The white boxes represent the enlarged areas. Magnification: 20X; scale bar: 100 μm. **(J)** Statistical analysis of FPN expression in the neurons of each group. **(K–N)** Immunofluorescence staining of NeuN (green), TFH (purple), and DAPI (blue) in each group at 7 d.p.i. K_1–N_3 represent the enlarged images. K_2–N_2/K_3–N_3 represent the green and purple single-channel images of K_1–N_3, respectively. K_1–N_1 represent the merged images of each single channel. The white boxes represent the enlarged areas. Magnification: 20X; scale bar: 100 μm. **(O)** Statistical analysis of TFH expression in the neurons of each group. **(P–S)** Immunofluorescence staining of NeuN (green), FTL (purple), and DAPI (blue) in each group at 7 d.p.i. P_1–S_3 represent the enlarged images. P_2–S_2/P_3–S_3 represent the green and purple single-channel images of P_1–S_3, respectively. P_1–S_1 represent the merged images of each single channel. The white boxes represent the enlarged areas. Magnification: 20X; scale bar: 100 μm. **(T)** Statistical analysis of FTL expression in the neurons from each group. **(U)** Western blotting showing the expression of TFR, FPN, FTH and FTL in each group (tissue) at 7 d.p.i. **(V–Y)** Quantitative analysis of TFR **(V)**, FPN **(W)**, FTH **(X)** and FTL **(Y)** protein expression. ** represents $P < 0.01$ vs. the SCI group. ## represents $P < 0.01$. The data are represented as the mean ± SD ($n = 6$).

the ferroptosis of neurons by 1). reducing iron transport into cells and the storage of iron ions by downregulating TFR, FTH and FTL, 2). increasing the transport of iron ions outside the cell by upregulating FPN. The better effect of the hydrogel combined with DPSCs is related to the effect of DPSCs on vascular regulation.

18.5. The TPA@laponite shear-thinning hydrogel combined with DPSCs effectively promoted the recovery of motor function in mice with SCI

The motor function of mice was evaluated 1, 3, 7, 10, 14, 21 and 30 d.p.i. As observed in the footstep imprinting experiment, severe imprinting disorder with a wave shape and dragged movement were observed in the mice from the SCI group, Gel group and Gel + DPSC group. After Gel + DPSC hydrogel treatment, despite the disordered footstep imprinting, off-ground movement of the hind limbs was clearly observed (Fig. 5A). A higher BMS score was observed in the Gel + DPSC hydrogel-treated animals compared with the other injured animals (Fig. 5B). The hindlimb movement of the mice was also analyzed. In the mice of the SCI group, the connection lines of hindlimb joints were approximately horizontal and straight, and few joint movements of the lower limb were observed. The hind limb joints of the hydrogel-treated mice could move but were not strong enough to support their weight. However, the hind limb joints of the mice treated with the hydrogel combined with DPSCs could support their body weight, and some of these mice could not frequently move the front and rear limbs together (Fig. 5C). According to quantitative analysis, a more effective plantar support range (Fig. 5D), higher maximum height from the ground (Fig. 5E) and shorter spasm duration (Fig. 5F) were observed in the mice treated with the hydrogel combined with DPSCs compared with the hydrogel-treated mice and the mice with SCI, indicating an improvement in the motor function of murine hindlimbs after treatment with the hydrogel combined with DPSCs. EMG of mice showed that the time required for nerve impulse transfer from the damaged section to the gastrocnemius was significantly prolonged and that the energy contained in the impulse was significantly reduced after SCI. Treatment with the hydrogel alone promoted recovery, and treatment with the TPA@Laponite hydrogel combined with dental pulp stem cells exerted a synergistic effect that promoted the recovery of bioelectrical conduction in the mice with SCI (Fig. 5G).

In conclusion, the TPA@lapnoite shear-thinning hydrogel combined with DPSCs effectively promoted the recovery of motor function in mice with SCI.

18.6. The TPA@laponite shear-thinning hydrogel combined with DPSCs promoted SCI recovery by regulating the ratio of inhibitory and excitatory neurons

The recovery of motor function after spinal cord injury is closely related to the regeneration of axons [46,47]. The expression of NF200, which indicates axon regeneration, was measured by immunofluorescence, and the results showed upregulated expression across the glial scar in the Gel + DPSC group (Sfigure 8A-B). The distance between both sides of the glial scars was the smallest in the Gel + DPSC group (Sfigure 8A, C). Furthermore, the results indicated that the diameter of regenerated axons within the areas both inside and outside the glial scar was larger in the Gel + DPSC group than in the SCI group and the Gel groups (Sfigure 8D-E). In our ethology studies, we found that the animals from the SCI group had a longer spasm duration, but the animals from the Gel group and Gel + DPSC group did not. To determine the cause of this phenomenon, we analyzed the types of spinal lamellar IV neurons that regulate articular muscle movement (α-Motor neurons are equipped with extraspindle muscle fibers across joints to regulate joint movement, and γ-motor neurons are equipped with interspindle muscle fibers to regulate muscle tension). Our results showed more GABA-capable synapses and fewer glutamate synapses around α neurons and γ neurons in the Sham group (Fig. 6A, E). After SCI, a large number of neurons died, and decreased numbers of GABA-capable synapses and increased numbers of glutamate synapses were observed in the spinal cord (Fig. 6B, F). In the Gel group, some viable neurons were observed in the damaged area. Compared with the Sham group, the number of GABA-capable synapses around α neurons and γ neurons decreased in the TPA group, while that of glutamate-capable synapses increased (Fig. 6C, G). We also found an increased number of GABAergic synapses around α neurons and γ neurons and a decreased number of glutamate synapses in the Gel + DPSC group compared with the Gel group (Fig. 6D, H). To further verify the regulatory effect of the TPA@Laponite hydrogel combined with DPSCs on types of synapses, we conducted a series of *in vitro* experiments. We first identified DPSCs based on STRO-1, CD90 and CD34 expression, and the experimental results showed that the cells we extracted were DPSCs (Sfigure 9A-D). Then, we observed the differentiation of these cells after culture in neural differentiation medium and in the presence of the hydrogel. The experimental results showed that DPSCs could express ASCL1 and differentiate into neurons. After hydrogel treatment, the expression of ASCL1 in dental pulp stem cells and the rate of neuron differentiation were significantly increased (Sfigure 9E-M).

In conclusion, the hydrogel combined with DPSCs could increase the number of GABA-induced synapses and decrease the number of glutamate-induced synapses to reduce hyperexcitation-induced muscle spasms.

19. Discussion

The spinal cord is a pivotal part of the CNS. The spinal cord is a soft tissue, and its morphology changes following the movement of the spine [48]. Cells in the spinal cord are relatively fragile and vulnerable to damage and/or death when exposed to external forces [49,50]. Therefore, the hydrogels used in the treatment of SCI need to be soft. For shear-thinning hydrogels, their rigidity gradually decreases under the action of shear force [51,52]. Laponite is a common shear-thinning hydrogel gelling agent with a positively charged edge and a negatively charged surface [53,54]. In this study, the positively charged TPA and

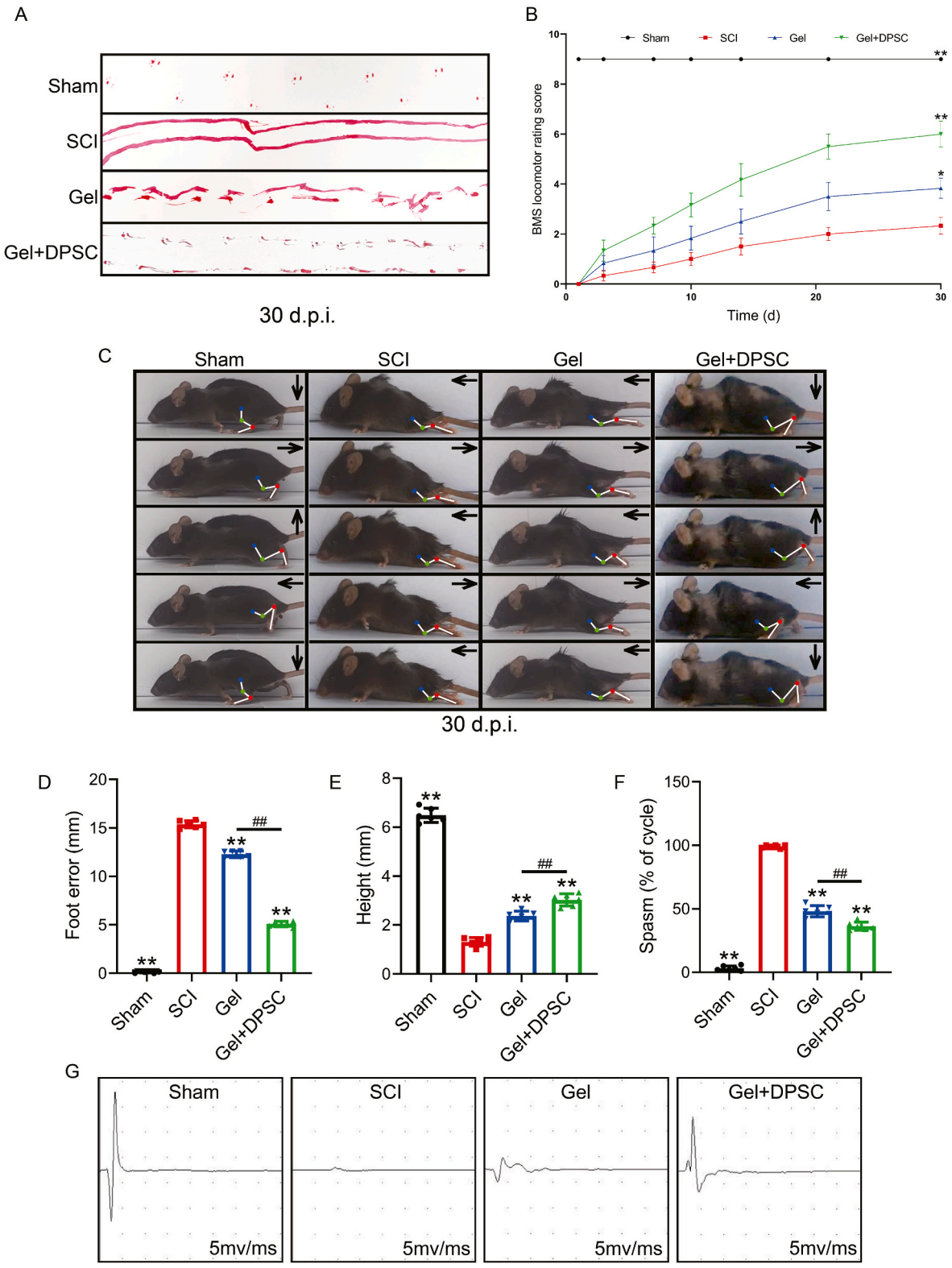

Fig. 5. The TPA@laponite shear-thinning hydrogel combined with DPSCs promotes the recovery of motor function in mice with SCI
(A) The gait marks of the mice in each group at Day 30. **(B)** BMS score of mice at the corresponding time points. **(C)** High-frame rate camera image showing the motion of the mice in each group. The dots represent the leg joints of the mouse, and the white lines are the connections between the joints. **(D–F)** Statistical analysis of hind limb motor function of the mice, including **(D)** foot error, **(E)** height and **(F)** spasm. **(G)** Electrophysiological measurement of each group at Day 30. In the figure, each small space in the horizontal direction represents 1 ms, and each small space in the vertical direction represents 5 mV. The data are expressed as the mean values ± SDs, n = 6. * represents $P < 0.05$ and ** represents $P < 0.01$ vs. the SCI group. # represents $P < 0.05$, and ## represents $P < 0.01$. The data are represented as the mean ± SD (n = 6).

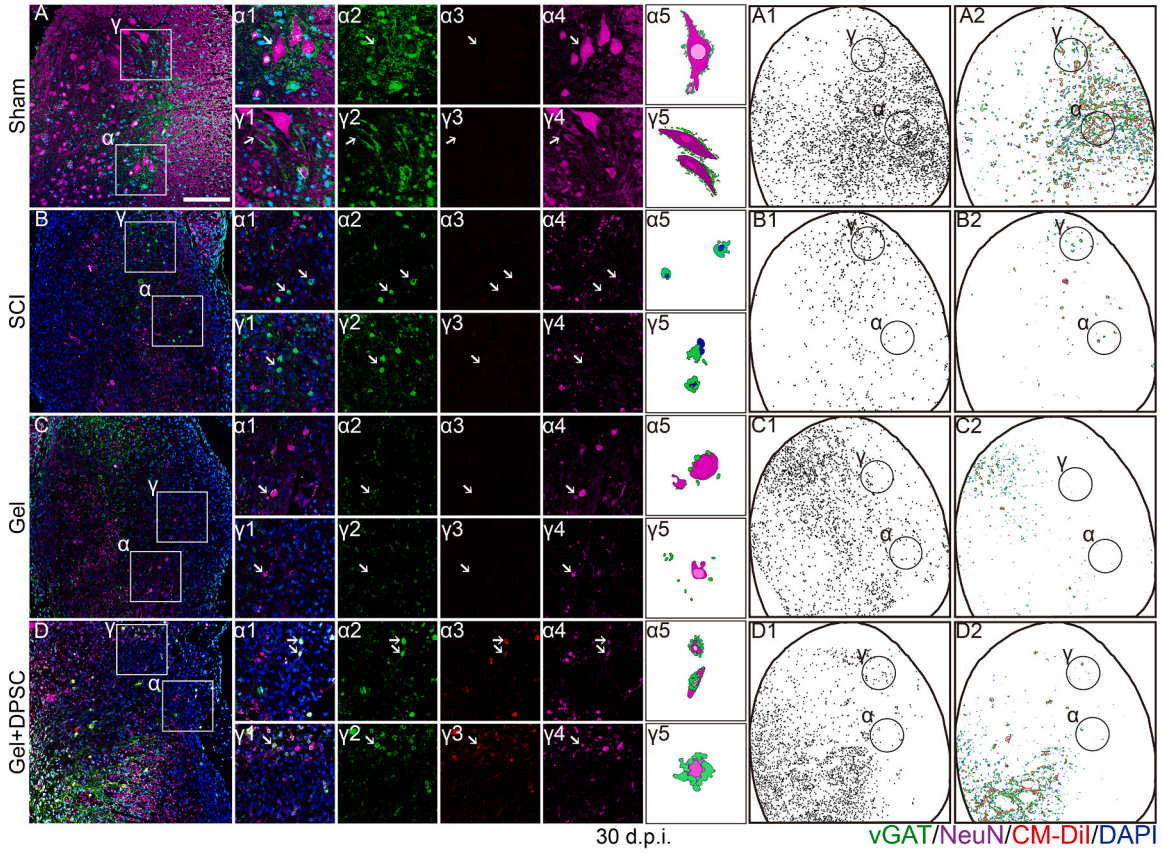

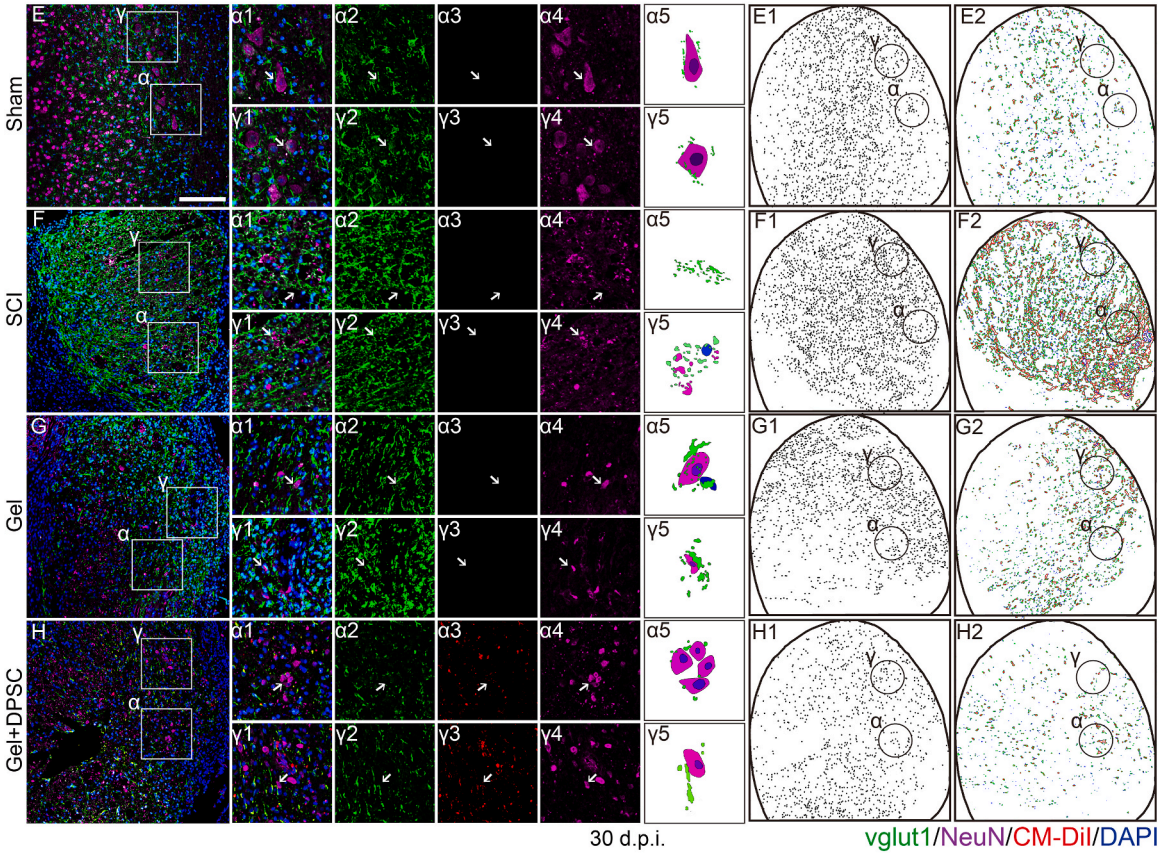

(caption on next page)

Fig. 6. The TPA@laponite shear-thinning hydrogel combined with DPSCs regulates the ratio of inhibitory and excitatory neurons
(A- H) Immunofluorescence staining of GAT **(green, A-D)**/vglut1 **(green, F–H)**, NeuN (purple), CM-Dil (red) and DAPI (blue) in each group. Higher magnification images of the α and γ regions are displayed. The α and γ regions contain α motor neurons and γ sensory neurons, respectively. α_1 represents an enlarged image of the α region. γ_1 represents an enlarged image of the γ region. $\alpha_{2\text{-}4}$ represent the green, red and purple single-channel images of α1, respectively. $\gamma_{2\text{-}4}$ represent the green, red and purple single-channel images of γ_1, respectively. α_5 and γ_5 are diagrams of typical neuron patterns in each area. The arrow indicates the position of the corresponding cell in the patterns. A1-D1/E1-H1 represent the scatter plot of GAT^+/$vglut1^+$ cells with the interference of DAPI excluded. A2-D2/E2-H2 represents the s contour plot of GAT^+ cells with the interference of DAPI excluded. The red line represents the contour with a density of 50. The green line represents the contour with a density of 35. The blue line represents the contour with a density of 30. Magnification: 20X; scale bar: 100 μm.

negatively charged Laponite surface were combined to form a TPA@-laponite shear-thinning hydrogel (Fig. 1; SFigs. 1 and 2). Compared with Zhao et al.'s TPA@PVA hydrogel, the TPA@Laponite hydrogel has better deformation ability and is more suitable for the treatment of SCI [27].

ROS-scavenging hydrogels have been explored for use in tissue regeneration [55,56]. In this study, our *in vitro* and *in vivo* data showed that the TPA@Laponite hydrogel had scavenged ROS well and inhibited lipid peroxidation, which confirmed that the TPA@Laponite hydrogel could play a particular role in the protection of stem cells during cell transplantation (Figs. 2–3). Interestingly, we also found that iron metabolism in cells and tissues was regulated by the TPA@Laponite hydrogel (Fig. 4). In the process of ferroptosis, iron ions are transported into the cell by TFR to induce a Fenton reaction, which produces a large

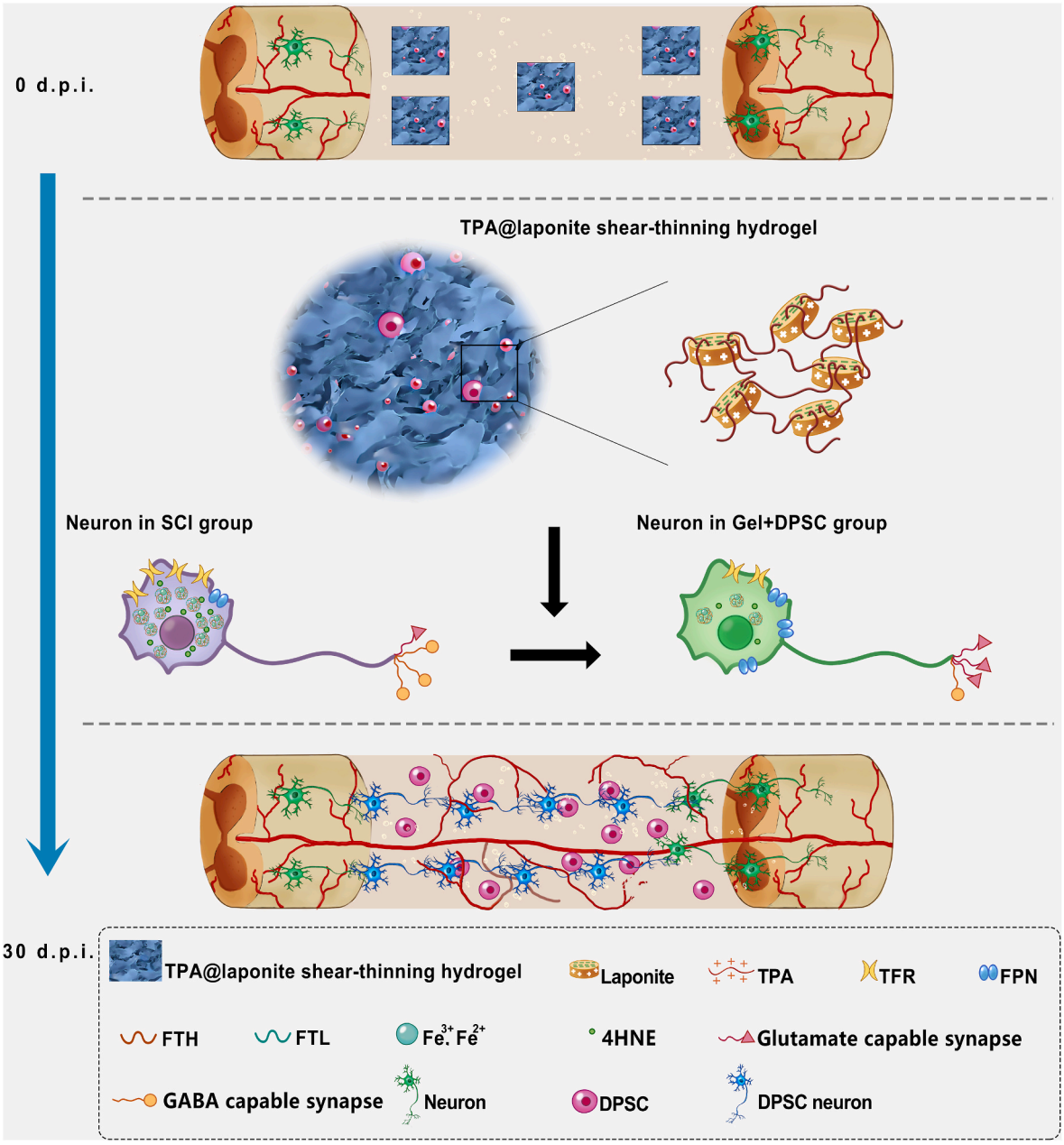

Fig. 7. Diagram of the mechanism by which the shear-thinning hydrogel that scavenges ROS combined with dental pulp stem cells repair spinal cord injury by inhibiting ferroptosis.

number of lipid peroxides, and the expression of FPN is downregulated to reduce iron extracellular transport; however, ferrous ions have no such effect [57–59]. The intracellular expression of FTH and FTL, which are components of ferritin, is also affected by iron ions, and FTH converts iron ions into ferrous ions to reduce the cell death caused by iron overload [60]. Hydrogels composed of TPA scavenge ROS and exert certain reduction effects [27,61]. TPA@Laponite hydrogel can convert iron ions into ferrous ions in the extracellular space and reduce the extracellular iron ion level to alleviate iron overload (Figs. 3 and 6).

In our study, we found that the Gel + DPSC group achieved better therapeutic results than the Gel group. The mechanism by which the TPA@lapnoite shear-thinning hydrogel combined with DPSCs synergistically regulates iron metabolism attracted our attention. When the body's iron homeostasis is disrupted, iron ions will be transported to the cell or transported to the liver through blood vessels for metabolism [62,63]. The iron ion absorption capacity of local cells is limited, and excessive iron ions lead to cell iron overload and cell death [64,65]. Therefore, the vascular transport of iron ions is an important way to regulate iron homeostasis. Mechanical injury after spinal cord injury leads to vascular rupture, and it is difficult for iron ions to be transported out of the site of injury [66,67]. Although the TPA@Laponite hydrogel can reduce iron ion levels and relieve the pressure of iron overload, a large amount of oxygen free radicals is generated in the site of injury after SCI, which can oxidize ferrous ions. The TPA@Laponite hydrogel can only reduce the entanglement of vascular and fibrous scars but cannot effectively promote the recovery of vascular function. DPSCs can differentiate into both nerves and blood vessels. Previous studies have found that DPSCs have a significant effect on the recovery of vascular function. In this study, we confirmed that DPSCs can significantly reduce the formation of fibrous scars and promote the recovery of vascular function, which leads to the synergism of the TPA@Laponite hydrogel and DPSCs in regulating iron metabolism (SFig. 7).

Furthermore, we also found that the mice in the SCI group exhibited few hind limb movements, while the mice from the Gel group and the Gel + DPSC group exhibited some rotation, with the mice from the Gel group showing a longer time of spasm (Fig. 5). VGAT is an indicator of synapses in GABA-capable neurons that inhibit downstream neurons. Vglut1 is an indicator of synapses in glutamate-capable neurons that promote the excitability of downstream neurons. Our results showed that vGAT decreased and vglut1 increased after SCI. Laminar IX controls muscle movement, with α motor neurons regulating cross-joint movement and γ motor neurons regulating muscle tone [68]. Our results showed that almost no motor neurons survived in the SCI group. In the Gel group, although some motor neurons survived, the corresponding synapses on neurons changed, including decreased vGAT and increased vglut1. In the Gel + DPSC group, DPSCs differentiated into motor neurons and integrated into neural circuits. The expression of vGAT around the motor neurons was higher than that in the Gel group, and the expression of excitatory and inhibitory neurons was similar to that of the Sham group. vglut1, which is a marker of excitatory synapses, was expressed at low levels in the peripheral motor neurons of the TD group, which was similar to the Sham group. The evidence strongly suggests that spasticity in neuron recovery after SCI occurs due to an increased number of excitatory synapses and a decreased number of inhibitory synapses. Compared with the TPA@lapnoite shear-thinning hydrogel, the TPA@lapnoite shear-thinning hydrogel plus DPSCs was more efficient in regenerating GABA-capable synapses and inhibiting glutamate capable synapses. This effect is related to the promotion of ASCL1 expression by the TPA@Laponite hydrogel (Fig. 6; SFig. 9). ASCL1 has been reported in many studies to promote the differentiation of stem cells into GABAergic neurons [69,70].

In summary, we designed a TPA@Laponite shear-thinning hydrogel that conforms to the physiological nature of the spinal cord. Due to the ability of the hydrogel to scavenge ROS and the ability of DPSCs to repair vascular function, the TPA@laponite hydrogel combined with DPSCs synergistically regulates iron metabolism to inhibit ferroptosis and promote the recovery of spinal cord iron homeostasis. Furthermore, this material can regulate the regeneration of synapses, subsequently reducing the extent of muscle spasm (Fig. 7).

Ethics approval and consent to participate

All protocols and animal experiments were conducted in strict accordance with the Animal Care and Use Committee of Wenzhou Medical University (No. WYDW-2018- 0342).

All protocols of collection and application of human dental pulp stem cells were approved by ethical committee of Wenzhou Medical University (No. WYKQ2018008SC).

CRediT authorship contribution statement

Yibo Ying: coordinated and carried out most of the experiments and data analysis and participated in drafting the manuscript. **Zhiyang Huang:** coordinated and carried out most of the experiments and data analysis and participated in drafting the manuscript. **Yurong Tu:** coordinated and carried out most of the experiments and data analysis and participated in drafting the manuscript. **Qiuji Wu:** coordinated and carried out most of the experiments and data analysis and participated in drafting the manuscript. **Zhaoyu Li:** carried out assistance on data analysis and manuscript preparation. **Yifan Zhang:** provided technical assistance. **Huilei Yu:** provided technical assistance. **Annian Zeng:** provided technical assistance. **Hanzhi Huang:** provided technical assistance. **Jiahui Ye:** provided technical assistance. **Weiyang Ying:** carried out assistance on data analysis and manuscript preparation. **Min Chen:** carried out assistance on data analysis and manuscript preparation. **Zhiyi Feng:** carried out assistance on data analysis and manuscript preparation. **Ziyue Xiang:** carried out assistance on data analysis and manuscript preparation. **Qingsong Ye:** obtained the ethics approval of using human DPSC and provided expertise in applying DPSC, supervised the project and revised the manuscript. **Sipin Zhu:** supervised the project and experimental designs and data analysis, supervised the project and revised the manuscript. **Zhouguang Wang:** supervised the project and experimental designs and data analysis, supervised the project and revised the manuscript, All authors approved the final manuscript.

Declaration of competing interest

The authors declare no competing interests.

Acknowledgements

This study was partly funded by grants from the National Natural Science Funding of China (82172424, 82271629), Outstanding Youth Fund of Zhejiang Province (LR22H060002), Zhejiang Medical and Health Science and Technology Plan Project (2022RC210, 2021KY212), and Wenzhou Basic Science Research Plan Project (Y20210045), CAMS Innovation Fund for Medical Sciences (2019-I2M-5–028).

Appendix A. Supplementary data

Supplementary data to this article can be found online at https://doi.org/10.1016/j.bioactmat.2022.09.019.

References

[1] Global, regional, and national burden of traumatic brain injury and spinal cord injury, A systematic analysis for the global burden of disease study 2016, the lancet, Neurology 18 (1) (1990-2016) 56–87, https://doi.org/10.1016/s1474-4422(18)30415-0.

[2] F. Geisler, W. Coleman, E. Benzel, et al., Spinal cord injury, Lancet (London, England) 360 (9348) (1883), https://doi.org/10.1016/s0140-6736(02)11744-2 author reply 1884.

[3] L. Ramer, M. Ramer, and E. Bradbury, Restoring function after spinal cord injury: towards clinical translation of experimental strategies, Lancet Neurol. 13(12) 1241-1256. 10.1016/s1474-4422(14)70144-9.
[4] P. Assinck, G. Duncan, B. Hilton, et al., Cell transplantation therapy for spinal cord injury, Nat. Neurosci. 20(5) 637-647. 10.1038/nn.4541.
[5] Y. Li, X. He, R. Kawaguchi, et al., Microglia-organized scar-free spinal cord repair in neonatal mice, Nature. 587(7835) 613-618. 10.1038/s41586-020-2795-6.
[6] A. Sas, K. Carbajal, A. Jerome, et al., A new neutrophil subset promotes CNS neuron survival and axon regeneration, Nat. Immunol. 21(12) 1496-1505. 10.1038/s41590-020-00813-0.
[7] S. Gronthos, M. Mankani, J. Brahim, et al., Postnatal human dental pulp stem cells (DPSCs) in vitro and in vivo, Proc. Natl. Acad. Sci. U. S. A. 97(25) 13625-13630.
[8] X. Shi, J. Mao, and Y. Liu, Pulp stem cells derived from human permanent and deciduous teeth: biological characteristics and therapeutic applications, Stem Cells Transl. Med.. 9(4) 445-464. 10.1002/sctm.19-0398.
[9] N. Nuti, C. Corallo, B. M. F. Chan, et al., Multipotent differentiation of human dental pulp stem cells: a literature review, Stem Cell Rev. Rep.. 12(5) 511-523.
[10] F. Ferro, R. Spelat, and C. S. Baheney, Dental pulp stem cell (DPSC) isolation, characterization, and differentiation, Methods Mol. Biol.. 1210. 10.1007/978-1-4939-1435-7_8.
[11] E. P. Chalisserry, S. Y. Nam, S. H. Park, et al., Therapeutic potential of dental stem cells, J. Tissue Eng.. 8 2041731417702531. 10.1177/2041731417702531.
[12] X. Yang, L. Li, L. Xiao, et al., Recycle the dental fairy's package: overview of dental pulp stem cells, Stem Cell Res. Ther.. 9(1) 347. 10.1186/s13287-018-1094-8.
[13] Z.-W. Li, J.-J. Li, L. Wang, et al., Epidermal growth factor receptor inhibitor ameliorates excessive astrogliosis and improves the regeneration microenvironment and functional recovery in adult rats following spinal cord injury, J. Neuroinflammation 11 71. 10.1186/1742-2094-11-71.
[14] L. Li, B. Xiao, J. Mu, et al., A MnO nanoparticle-dotted hydrogel promotes spinal cord repair regulating reactive oxygen species microenvironment and synergizing with mesenchymal stem cells, ACS Nano. 13(12) 14283-14293. 10.1021/acsnano.9b07598.
[15] X. Ding, J. Gao, Z. Wang, et al., A shear-thinning hydrogel that extends in vivo bioactivity of FGF2, Biomaterials. 111 80-89. 10.1016/j.biomaterials.2016.09.026.
[16] L. Fan, C. Liu, X. Chen, et al., Directing induced pluripotent stem cell derived neural stem cell fate with a three-dimensional biomimetic hydrogel for spinal cord injury repair, ACS Appl. Mater. Interfaces. 10(21) 17742-17755. 10.1021/acsami.8b05293.
[17] N. Zandi, E. Sani, E. Mostafavi, et al., Nanoengineered shear-thinning and bioprintable hydrogel as a versatile platform for biomedical applications, Biomaterials. 267 120476. 10.1016/j.biomaterials.2020.120476.
[18] R. Hirose, T. Nakaya, Y. Naito, et al., Performance comparison between next-generation and shear-thinning hydrogel-based submucosal injection materials, Gastrointest. Endosc. 93(3) 777-779.e4. 10.1016/j.gie.2020.10.030.
[19] M. Arkenberg, H. Nguyen, and C. Lin, Recent advances in bio-orthogonal and dynamic crosslinking of biomimetic hydrogels, J. Mater. Chem. B. 8(35) 7835-7855. 10.1039/d0tb01429j.
[20] E. Alarçin, T. Lee, S. Karuthedom, et al., Injectable shear-thinning hydrogels for delivering osteogenic and angiogenic cells and growth factors, Biomater. Sci.. 6(6) 1604-1615. 10.1039/c8bm00293b.
[21] A. Masood, N. Sarika, B. Heather A.E, et al., Skin biomechanics: breaking the dermal barriers with microneedles, Nano TransMed.. 1(1) e9130002. 10.26599/NTM.2022.9130002.
[22] Y. Shin, R. Shafranek, J. Tsui, et al., 3D bioprinting of mechanically tuned bioinks derived from cardiac decellularized extracellular matrix, Acta Biomater.. 119 75-88. 10.1016/j.actbio.2020.11.006.
[23] H. Tomás, C. Alves, and J. Rodrigues, Laponite®: a key nanoplatform for biomedical applications?, Nanomed. Nanotechnol. Biol. Med.. 14(7) 2407-2420. 10.1016/j.nano.2017.04.016.
[24] X. Tong and F. Yang, Recent progress in developing injectable matrices for enhancing cell delivery and tissue regeneration, Adv. Healthc. Mater.. 7(7) e1701065. 10.1002/adhm.201701065.
[25] Y. Pang, J. Liu, Z. Moussa, et al., Endoscopically injectable shear-thinning hydrogels facilitating polyp removal, Adv. Sci.. 6(19) 1901041. 10.1002/advs.201901041.
[26] Y. Keum, B. Kim, A. Byun, et al., Synthesis and photocatalytic properties of titanium-porphyrinic aerogels, Angew. Chem.. 59(48) 21591-21596. 10.1002/anie.202007193.
[27] H. Zhao, J. Huang, Y. Li, et al., ROS-scavenging hydrogel to promote healing of bacteria infected diabetic wounds, Biomaterials. 258 120286. 10.1016/j.biomaterials.2020.120286.
[28] Y. Sun, P. Chen, B. Zhai, et al., The emerging role of ferroptosis in inflammation, Biomed. Pharmacother.. 127 110108. 10.1016/j.biopha.2020.110108.
[29] T. Hirschhorn and B. R. Stockwell, The development of the concept of ferroptosis, Free Radic. Biol. Med.. 133 130-143. 10.1016/j.freeradbiomed.2018.09.043.
[30] W. S. Yang and B. R. Stockwell, Ferroptosis: death by lipid peroxidation, Trends Cell Biol.. 26(3) 165-176. 10.1016/j.tcb.2015.10.014.
[31] K. Bersuker, J. M. Hendricks, Z. Li, et al., The CoQ oxidoreductase FSP1 acts parallel to GPX4 to inhibit ferroptosis, Nature. 575(7784) 688-692. 10.1038/s41586-019-1705-2.
[32] K. Rathore, B. Kerr, A. Redensek, et al., Ceruloplasmin protects injured spinal cord from iron-mediated oxidative damage, J. Neurosci. : Off. J. Soc. Neurosci.. 28(48) 12736-12747. 10.1523/jneurosci.3649-08.2008.
[33] G. Guangzhao, H. Yan, and M. Li, Atomic force microscopy: a nanobiotechnology for cellular research, Nano TransMed.. 1(1) e9130004. 10.26599/NTM.2022.9130004.
[34] X. Yang, R. Yang, M. Chen, et al., KGF-2 and FGF-21 poloxamer 407 hydrogel coordinates inflammation and proliferation homeostasis to enhance wound repair of scalded skin in diabetic rats, BMJ Open Diab. Res. Care. 8(1). 10.1136/bmjdrc-2019-001009.
[35] Y. Li, R. M. Ritzel, N. Khan, et al., Delayed microglial depletion after spinal cord injury reduces chronic inflammation and neurodegeneration in the brain and improves neurological recovery in male mice, Theranostics. 10(25) 11376-11403. 10.7150/thno.49199.
[36] S. P. Zhu, Y. B. Ying, Q. J. Wu, et al., Alginate self-adhesive hydrogel combined with dental pulp stem cells and FGF21 repairs hemisection spinal cord injury via apoptosis and autophagy mechanisms, Chem. Eng. J.. 426. ARTN 130827. 10.1016/j.cej.2021.130827.
[37] H. Duan, Y. Pang, C. Zhao, et al., A novel, minimally invasive technique to establish the animal model of spinal cord injury, Ann. Transl. Med.. 9(10) 881. 10.21037/atm-21-2063.
[38] Y. Hu, J. Wu, X. Zhang, et al., Effects of paired associative stimulation on metabolites in ischemia stroke rats model as studied by nuclear magnetic resonance spectrum, Neurochem. Res.. 46(9) 2495-2504. 10.1007/s11064-021-03388-w.
[39] Y. Gong, N. Wang, N. Liu, et al., Lipid peroxidation and GPX4 inhibition are common causes for myofibroblast differentiation and ferroptosis, DNA Cell Biol.. 38(7) 725-733. 10.1089/dna.2018.4541.
[40] R. Shintoku, Y. Takigawa, K. Yamada, et al., Lipoxygenase-mediated generation of lipid peroxides enhances ferroptosis induced by erastin and RSL3, Cancer Sci.. 108 (11) 2187-2194. 10.1111/cas.13380.
[41] A. Donovan, C. A. Lima, J. L. Pinkus, et al., The iron exporter ferroportin/Slc40a1 is essential for iron homeostasis, Cell Metabol.. 1(3) 191-200. 10.1016/j.cmet.2005.01.003.
[42] H. Kawabata, Transferrin and transferrin receptors update, Free Radic. Biol. Med.. 133 46-54. 10.1016/j.freeradbiomed.2018.06.037.
[43] X. Fang, Z. Cai, H. Wang, et al., Loss of cardiac ferritin H facilitates cardiomyopathy via slc7a11-mediated ferroptosis, Circ. Res.. 127(4) 486-501. 10.1161/CIRCRESAHA.120.316509.
[44] Z. Feng, L. Min, H. Chen, et al., Iron overload in the motor cortex induces neuronal ferroptosis following spinal cord injury, Redox Biol.. 43 101984. 10.1016/j.redox.2021.101984.
[45] X. Hu, Y. Xu, H. Xu, et al., Progress in understanding ferroptosis and its targeting for therapeutic benefits in traumatic brain and spinal cord injuries, Front. Cell Dev. Biol.. 9 705786. 10.3389/fcell.2021.705786.
[46] M. Anderson, T. O'Shea, J. Burda, et al., Required growth facilitators propel axon regeneration across complete spinal cord injury, Nature. 561(7723) 396-400. 10.1038/s41586-018-0467-6.
[47] F. Li, A. Sami, H. Noristani, et al., Glial metabolic rewiring promotes axon regeneration and functional recovery in the central nervous system, Cell Metabol.. 32(5) 767-785.e7. 10.1016/j.cmet.2020.08.015.
[48] M. Walker, Acute spinal-cord injury, N. Engl. J. Med.. 324(26) 1885-1887. 10.1056/nejm199106273242608.
[49] L. Galluzzi, J. Bravo-San Pedro, K. Blomgren, et al., Autophagy in acute brain injury, Nat. Rev. Neurosci. 17(8) 467-484. 10.1038/nrn.2016.51.
[50] A. Tran, P. Warren, and J. Silver, The biology of regeneration failure and success after spinal cord injury, Physiol. Rev. 98(2) 881-917. 10.1152/physrev.00017.2017.
[51] A. Sisso, M. Boit, and C. DeForest, Self-healing injectable gelatin hydrogels for localized therapeutic cell delivery, J. Biomed. Mater. Res. A. 108(5) 1112-1121. 10.1002/jbm.a.36886.
[52] P. Ren, J. Li, L. Zhao, et al., Dipeptide self-assembled hydrogels with shear-thinning and instantaneous self-healing properties determined by peptide sequences, ACS Appl. Mater. Interfaces. 12(19) 21433-21440. 10.1021/acsami.0c03038.
[53] C. Tondera, T. Akbar, A. Thomas, et al., Highly conductive, stretchable, and cell-adhesive hydrogel by nanoclay doping, Small. 15(27) e1901406. 10.1002/smll.201901406.
[54] J. Dawson, J. Kanczler, X. Yang, et al., Clay gels for the delivery of regenerative microenvironments, Adv. Mater.. 23(29) 3304-3308. 10.1002/adma.201100968.
[55] Y. Guan, H. Niu, Z. Liu, et al., Sustained oxygenation accelerates diabetic wound healing by promoting epithelialization and angiogenesis and decreasing inflammation, Sci. Adv.. 7(35). 10.1126/sciadv.abj0153.
[56] J. Zhou, W. Liu, X. Zhao, et al., Natural melanin/alginate hydrogels achieve cardiac repair through ROS scavenging and macrophage polarization, Adv. Sci. 8(20) e2100505. 10.1002/advs.202100505.
[57] B. R. Stockwell, X. Jiang, and W. Gu, Emerging mechanisms and disease relevance of ferroptosis, Trends Cell Biol.. 30(6) 478-490. 10.1016/j.tcb.2020.02.009.
[58] A. Ashraf, J. Jeandriens, H. G. Parkes, et al., Iron dyshomeostasis, lipid peroxidation and perturbed expression of cystine/glutamate antiporter in Alzheimer's disease: evidence of ferroptosis, Redox Biol.. 32 101494. 10.1016/j.redox.2020.101494.
[59] Y. J. He, X. Y. Liu, L. Xing, et al., Fenton reaction-independent ferroptosis therapy via glutathione and iron redox couple sequentially triggered lipid peroxide generator, Biomaterials. 241 119911. 10.1016/j.biomaterials.2020.119911.
[60] D. C. Fuhrmann, A. Mondorf, J. Beifuss, et al., Hypoxia inhibits ferritinophagy, increases mitochondrial ferritin, and protects from ferroptosis, Redox Biol.. 36 101670. 10.1016/j.redox.2020.101670.
[61] Y. Li, J. Wang, Y. Yang, et al., A rose bengal/graphene oxide/PVA hybrid hydrogel with enhanced mechanical properties and light-triggered antibacterial activity for wound treatment, Mater. Sci. Eng. C Mater. Biol. Appl.. 118 111447. 10.1016/j.msec.2020.111447.

[62] A. R. Bogdan, M. Miyazawa, K. Hashimoto, et al., Regulators of iron homeostasis: new players in metabolism, cell death, and disease, Trends Biochem. Sci.. 41(3) 274-286. 10.1016/j.tibs.2015.11.012.
[63] C. Y. Wang and J. L. Babitt, Liver iron sensing and body iron homeostasis, Blood. 133(1) 18-29. 10.1182/blood-2018-06-815894.
[64] L. Yang, H. Wang, X. Yang, et al., Auranofin mitigates systemic iron overload and induces ferroptosis via distinct mechanisms, Signal Transduct. Targeted Ther.. 5(1) 138. 10.1038/s41392-020-00253-0.
[65] M. E. Conrad and J. N. Umbreit, Iron absorption and transport-an update, Am. J. Hematol.. 64(4) 287-298. 10.1002/1096-8652(200008)64:4<287::aid-ajh9>3.0.co;2-l.
[66] E. A. Winkler, J. D. Sengillo, A. P. Sagare, et al., Blood-spinal cord barrier disruption contributes to early motor-neuron degeneration in ALS-model mice, Proc. Natl. Acad. Sci. U. S. A.. 111(11) E1035-E1042. 10.1073/pnas.1401595111.
[67] S. M. Sadrzadeh, D. K. Anderson, S. S. Panter, et al., Hemoglobin potentiates central nervous system damage, J. Clin. Invest.. 79(2) 662-664.
[68] C. D. MacKinnon, Sensorimotor anatomy of gait, balance, and falls, Handb. Clin. Neurol.. 159 3-26. 10.1016/B978-0-444-63916-5.00001-X.
[69] D. S. Soares, C. C. F. Homem, and D. S. Castro, Function of proneural genes Ascl1 and asense in neurogenesis: how similar are they?, Front. Cell Dev. Biol.. 10 838431. 10.3389/fcell.2022.838431.
[70] M. Chouchane and M. R. Costa, Instructing neuronal identity during CNS development and astroglial-lineage reprogramming: roles of NEUROG2 and ASCL1, Brain Res.. 1705 66-74. 10.1016/j.brainres.2018.02.045.